SUBMITTED TO THE PHYSICAL REVIEW
JUNE 11, 1979
E299

RU-79-152
FERMILAB-PUB-79-130-E

RECEIVED
JUL 5 1979
DIRECTORS OFFICE
FERMILAB

Inclusive Production of Neutral Strange Particles by 147 GeV/c $\pi^+/K^+/p$ Interactions in Hydrogen

D. Brick, A. M. Shapiro, and M. Widgoff
Brown University, Providence, Rhode Island 02912

R. E. Ansorge, J. R. Carter, W. W. Neale, J. G. Rushbrooke,
D. R. Ward, and B. M. Whyman
University of Cambridge, Cambridge, England

R. A. Burnstein and H. A. Rubin
Illinois Institute of Technology, Chicago, Illinois 60616

J. W. Cooper, R. L. Plumer, R. D. Sard, and J. O. Tortora[†]
University of Illinois, Urbana, Illinois 61801

E. D. Alyea
Indiana University, Bloomington, Indiana 47401

L. Bachman[*], C.-Y. Chien, and A. Pevsner
Johns Hopkins University, Baltimore, Maryland 21218

E. S. Hafen, D. Hochman, R. I. Hulsizer, V. Kistiakowsky,
A. Levy[§], P. Lutz[¶], I. A. Pless, P. Trepagnier, and R. K. Yamamoto
Massachusetts Institute of Technology, Cambridge, Massachusetts 02139

F. Grard, J. Hanton, V. Henri, P. Herquet, J. M. Lesceux, and R. Windmolders
Université de l'Etat, Mons, Belgium

H. deBock, F. Crijns, W. Metzger, C. Pols, M. Schouten, and R. Van de Walle
University of Nijmegen, Nijmegen, Netherlands

H. O. Cohn

Oak Ridge National Laboratory, Oak Ridge, Tennessee 37830

G. Bressi, E. Calligarich, C. Castoldi, G. Cecchet,

R. Dolfini, G. Liguori, and S. Ratti

University of Pavia and INFN, Pavia, Italy

P. F. Jacques, M. Kalelkar, R. J. Plano, P. Stamer, and T. L. Watts

Rutgers University, New Brunswick, New Jersey 08903

E. B. Brucker, E. L. Koller, and S. Taylor

Stevens Institute of Technology, Hoboken, New Jersey 07030

L. Berny, S. Dado, J. Goldberg, and S. Toaff

Technion, Haifa, Israel

G. Alexander, O. Benary, and J. Grunhaus

Tel-Aviv University, Tel-Aviv, Israel

W. M. Bugg, G. T. Condo, T. Handler, and E. L. Hart

University of Tennessee, Knoxville, Tennessee 37916

Y. Eisenberg, U. Karshon, E. E. Ronat, A. Shapira, R. Yaari, and G. Yekutieli

Weizmann Institute of Science, Rehovot, Israel

D. Ljung, T. Ludlam, and H. Taft

Yale University, New Haven, Connecticut 06520

†Present address: Dialog Systems, Belmont, Massachusetts

*Present address: Université de Neuchâtel, Neuchâtel, Switzerland

§On leave of absence from Tel-Aviv University, Tel-Aviv, Israel

¶On leave of absence from College De France, Paris, France

ABSTRACT

Results are presented from a study of inclusive neutral strange particle production by a 147 GeV/c tagged $\pi^+/K^+/p$ beam in the Fermilab 30-inch hydrogen bubble chamber. The experiment made use of the proportional hybrid spectrometer system. Results are based on 995 K_S°, 485 Λ, and 83 $\bar{\Lambda}$ found in a sample of 132,000 pictures. Cross sections are given for inclusive production of these particles by each of the three beam particles, and comparisons are made with measurements at other energies. Topological cross sections are also calculated, and KNO multiplicity scaling is investigated. Distributions are presented of invariant cross sections as functions of the Feynman scaling variable x and center of mass rapidity y. The transverse momentum-squared distributions with their fitted slopes are also given. Comparisons are made of the production characteristics for the three beam types.

I. Introduction

We have performed a study of inclusive neutral strange particle production by a tagged $\pi^+/K^+/p$ beam of 147 GeV/c momentum. The experiment was carried out in the Fermilab 30-inch hydrogen bubble chamber using the hybrid spectrometer system. In this paper we report results of the following reactions:

$$\pi^+ p \rightarrow K_s + \text{anything} \quad (1)$$

$$K^+ p \rightarrow K_s + \text{anything} \quad (2)$$

$$pp \rightarrow K_s + \text{anything} \quad (3)$$

$$\pi^+ p \rightarrow \Lambda + \text{anything} \quad (4)$$

$$K^+ p \rightarrow \Lambda + \text{anything} \quad (5)$$

$$pp \rightarrow \Lambda + \text{anything} \quad (6)$$

$$\pi^+ p \rightarrow \bar{\Lambda} + \text{anything} \quad (7)$$

$$K^+ p \rightarrow \bar{\Lambda} + \text{anything} \quad (8)$$

$$pp \rightarrow \bar{\Lambda} + \text{anything} \quad (9)$$

At high energies, neutral strange particle production has been studied in pp collisions at 100 GeV/c[1,2], 200 GeV/c[3,4], 300 GeV/c[5,6], and 400 GeV/c[7]. However, there is only one such study in π^+ collisions[1] and none in K^+p. This experiment represents the first attempt to measure inclusive production at Fermilab energies for all three types of beam particles in the same experiment. We are able to make comparisons among different beam types at the same energy with the same systematic errors.

In Section II of this paper we discuss the experimental apparatus and the beam, the scanning, measuring and reconstruction procedures, and the event selection criteria. In Section III we

give total inclusive cross sections for reactions (1) - (9). We also give topological cross sections for reactions (1) - (4) and (6). In Section IV we present inclusive distributions for all reactions. We show the invariant cross section

$$F_1(x) = \frac{2E^*}{\pi\sqrt{s}} \int \frac{d^2\sigma}{dx dP_T^2} dP_T^2$$

where the Feynman scaling variable $x = 2P_L^*/\sqrt{s}$, E^* is the energy of the produced particle in the center of mass, $\sqrt{s}$ is the total center of mass energy (about 16.6 GeV), P_T is the transverse momentum, and P_L^* is the longitudinal momentum of the produced particle in the center of mass. We also show the distributions of

$$G_1(y) = \int \frac{d^2\sigma}{dy dP_T^2} dP_T^2$$

where the center of mass rapidity y is given by

$$y = \frac{1}{2} \ln \frac{E^* + P_L^*}{E^* - P_L^*}$$

Finally, we present transverse momentum-squared distributions and their slopes.

II. Experimental Procedure

The experiment was performed in the Fermilab 30-inch hydrogen bubble chamber with proportional wire chambers (PWC) located both upstream and downstream. Details of this hybrid spectrometer system have been previously published[8,9]. Briefly, the upstream PWC's and a differential Cerenkov counter allowed tagging of π^+, K^+ and p in the incident beam. The downstream PWC's were used for

momentum measurements of fast forward particles from the primary vertex of an event. The downstream system also included a muon counter and a γ detector. The bubble chamber was enveloped by a 25 kilogauss magnetic field.

The beam consisted of 147 GeV/c positive particles. Two runs were made during the course of the experiment. In the first run, comprising 158,000 pictures, the composition of the beam was approximately 47% π^+, 4% K^+ and 49% p. In the second run of 240,000 picutres, the composition was 59% π^+, 10% K^+, and 31% p. There were an average of 6.5 beam tracks per frame. The results presented here are based on 132,000 frames, with contributions from both runs. The overall beam composition for events from the current sample is 47% π^+, 7% K^+, and 46% p. This is the first paper from this experiment (E299).

The film was scanned for all beam track interactions in a fiducial volume chosen to allow enough length for the beam to check its direction. Vertices of primary interactions and vees were digitized by scanners. Approximately 30% of the events were not measured, either because an excessive number of tracks entered the fiducial volume or because the frame contained more than two events. Events that were predigitized were subsequently measured by PEPR in a semi-automatic mode. The program GEOMAT was used to perform view-to-view track matching and space reconstruction. Reconstruction of tracks in the PWC's and beam track identification was done by the program PWGP. Correlation of bubble chamber and PWC information to obtain final track four vectors was performed by the program TKORG.

About 25% of the events in the first run, and 11% in the second run, were discarded because the beam track could not be identified by the existing PWC data. Of the remaining events, those which underwent measurement failures were remeasured (twice if necessary) in the entire sample of film reported here. A total of 18044 primary interactions were obtained, including 3976 neutral vees. Table I gives the number of events found for each beam type corrected for all detection losses, along with the corresponding microbarn equivalents, obtained by normalizing to the total inelastic cross sections.[10]

For the vees a minimum length cut of 3 cm in space from the primary vertex was imposed. In addition a decay volume was defined in such a way as to maximize the volume visible in all three views. This volume was bounded by ten planes, two of which were parallel to the front and back glass surfaces but displaced 5 cm into the chamber in order to provide adequate length for decay track measurement. The scan efficiency for finding neutrals was determined to be 91 ± 3% by doing a second scan on about 20% of the film.

Kinematic fitting of the vees to the primary vertex was accomplished with the program SQUAW. For each vee, three-constraint (3C) and 1C fits were attempted corresponding to the following hypotheses:

$$K_s \rightarrow \pi^+\pi^-$$

$$\Lambda \rightarrow p\pi^-$$

$$\bar{\Lambda} \rightarrow \bar{p}\pi^+$$

$$\gamma\ (p) \rightarrow (p)\ e^+e^-$$

A total of 3452 vees made successful 3C fits with a χ^2 less than 25. A much smaller number of vees (166) made 1C fits with χ^2 less than 5, but failed to make successful 3C fits. If there was an angular difference between the measured and fitted neutral of less than 60 milliradians, then the neutral was included in the final data sample. These vees failed the 3C fit because errors on the vertex coordinates were under-estimated by GEOMAT. Inclusion of these 1C fits did not appreciably alter the shapes of inclusive distributions. The quality of all fits was checked by examining χ^2 distributions and "pull" distributions of residual errors. These were found to have roughly the expected shapes for a correct assignment of errors.

Out of 3618 total fitted neutrals, there were 642 vees that had ambiguous fits. Table II gives the numbers of unambiguous and ambiguous fits. For about half of the ambiguous neutrals, the relative χ^2 probabilities differed by a factor of ten or greater, which permitted a clear resolution of the ambiguity. The transverse momentum spectrum of the decay tracks of strange particles with respect to the neutral line of flight is sharply peaked at the kinematic maximum. Since this distribution is peaked at zero for γ conversions, this quantity provides a clear separation of ambiguous fits. If the transverse momentum of the negative decay track was less than 20 MeV/c, the neutral was assigned to the γ sample; otherwise, the competing strange particle fit was chosen. The strange particle ambiguities were resolved by examining distributions of $\cos\theta_{cm}$, where θ_{cm} is the angle between the neutral line of flight and the direction of either decay product

in the rest frame of the neutral. For the spinless K_s, this distribution must be isotropic, and also isotropic for the Λ and $\bar{\Lambda}$ if they have no longitudinal polarization. Selections were made on relative χ^2 probability ratios in such a way as to render these decay angular distributions roughly isotropic. Figure 1 shows these distributions for the K_s and Λ. A further check was provided by examining the transverse momentum distributions of the negative decay track. These were found to have the expected shapes. We estimate that the K_s sample has about 6% contamination of Λ or $\bar{\Lambda}$; the Λ sample includes about 1% γ and about 8% K_s contamination. The contamination in the $\bar{\Lambda}$ sample is around 25%. The final sample consists of 995 K_s, 485 Λ, and 83 $\bar{\Lambda}$.

III. Total and Topological Cross Sections

As indicated in Table I the microbarn equivalents for the data sample were determined by normalizing the weighted numbers of events found for each beam type to the total inelastic cross section. To calculate the inclusive cross sections for neutral strange particles, each vee was weighted to account for scan inefficiency, measurement and geometry reconstruction losses, detection inefficiency due to the imposition of the minimum length cut and decay volume restriction, and neutral decay modes. However, no correction was made for the contribution from K_L, and no attempt was made to resolve the Λ-Σ° ambiguity. The average weight was 3.4 for K_s, and 3.3 for Λ. Table III gives the total inclusive cross section for each of the nine reactions studied in this experiment. The quoted errors include estimates of the uncertainty in each of the

corrections made, and the uncertainty in the procedure for resolving ambiguities, in addition to the statistical error.

In Figure 2 we compare our values of the total inclusive cross sections with data from other energies.[11] The K_s results are shown in Figure 2(a). Most other data at high energies come from pp experiments. Our result is in excellent agreement with the rising trend exhibited by the other experiments in the laboratory momentum range of 70-300 GeV/c. Our K_s cross section for π^+ agrees with an experiment[1] at 100 GeV/c which is the only measurement above 25 GeV/c. Data for K_s production in K^+p is only available up to 32 GeV/c. As indicated in Figure 2(a) these data show a much larger value for the cross section than for π^+p or pp, but a gentler energy dependence. Our value at 147 GeV/c is comparable to the pp cross section, but the error bars do not permit a meaningful quantitative comparison. Furthermore, there are systematic problems involved in detecting the fast-forward K° decays from diffractive beam dissociation. It is unlikely that the entire K_s cross section from K^+ has been measured. We will return to this point in Section IV.

Figure 2(b) shows results for the inclusive Λ. The pp data appear to level off above 70 GeV/c, a pattern that is confirmed by our experiment. Our value for π^+p is consistent with that for π^-p in this energy range. The K^+p results at lower energies indicate a rapidly rising cross section with energy. From 8 to 32 GeV/c the cross section rises by a factor of three. Our value at 147 GeV/c is about twice as large as the one at 32 GeV/c.

The inclusive $\bar{\Lambda}$ results are shown in Figure 2(c). Despite the large error bars, it is apparent that all the cross sections

are rising sharply. Furthermore, the inclusive $\bar{\Lambda}$ cross section appears to be around half the inclusive $\bar{p}$ production rate for pp collisions at energies above 50 GeV/c.[11] The $\bar{p}$ rate is indicated by the solid line in Figure 2(c). This result is in agreement with various constituent model predictions of strange quark pair production relative to non-strange production.[12] Our results are in agreement with this trend.

Tables IV and V give the topological cross sections by beam type for inclusive K_s and Λ production respectively. Figure 3 shows the average number of K_s and Λ per collision as a function of topology for reactions (1) - (4) and (6). In the cases of reactions (4) and (6), only those lambdas produced in the backward hemisphere in the center-of-mass system are included in Figure 3. The lines shown represent the best linear fits to the data. For reaction (2) the point at $n_{ch}=2$ has been omitted from the fit because of the loss of fast, forward, diffractive K_s. The slopes of all the fitted lines are consistent with zero; however, only the fits to Λ production yield reasonable χ^2, as shown. Therefore, it can be concluded that, within the experimental errors, Λ production is independent of charged particle multiplicity. This agrees with the hypothesis that Λ results primarily from target fragmentation while most of the charged particles are produced in the central region.

The result for K_s^o production can be contrasted with that for Λ. Although the slopes of the best linear fits to the K_s data are consistent with zero, the chi-squares are poor, and an examination of Figure 3 indicates that $\langle K_s^o \rangle_n$ does not fit to a straight line. The nature of this dependence is not clear, and the variation of

$\langle K_s^o \rangle_n$ with multiplicity is discussed in greater detail in reference 1.

The average number of Λ produced per inelastic collision in the backward hemisphere is the same, within experimental errors, for reactions (4) and (6), 0.06 ± 0.01 and 0.07 ± 0.01 respectively. This is consistent with the result in Figure 3, since target fragmentation should proceed in the same manner, regardless of beam type. However, the average number of K_s produced per inelastic collision is 0.15 ± 0.01 for the proton collisions, 0.21 ± 0.02 for the π^+ beam, and 0.21 ± 0.03 for the K^+ beam. For reaction (2), the K_s with rapidity > 1.5 have been excluded from this calculation in order to concentrate on central region production. This difference in $\langle K_s \rangle$ seems to indicate that the two mesons produce more K_s in the central region than do proton beams. This result has previously been observed in charged particle production by different beam types, although the effect was not as pronounced as it appears to be in K_s production. One explanation for the higher multiplicity of particles in meson collisions than that from proton beams may be derived from constituent model considerations. If multiparticle production is a result of constituent interactions, then the available energy of the constituents involved in a meson-proton collision is presumed to be higher than that for proton-proton collisions. Empirically it has been observed that average multiplicity increases with available energy. Therefore, one expects higher multiplicities from the more catastrophic meson-proton interactions. Another possible reason for the discrepancy is the contribution from the quark-antiquark annihilation process which is allowed in the meson interactions and absent in proton

collisions.

Figure 4 shows the topological cross sections plotted according to the semi-inclusive Koba-Nielsen-Olesen (KNO) scaling equation[14]

$$\frac{\langle n_c \rangle}{\langle n_v \rangle} \quad \frac{\sigma_n(V^\circ)}{\sigma_{inel.}} = \phi\left(\frac{n_c}{\langle n_c \rangle}\right)$$

where $\langle n_c \rangle$ and $\langle n_v \rangle$ are the average numbers of charged particles and vee particles respectively, $\sigma_n(v)$ is the inclusive topological cross section for production of the vee with n charged prongs, $\sigma_{inel.}$ is the total inelastic cross section, and ϕ is (presumably) an energy-independent function, as indicated in Figure 4.

Cohen has plotted results from pp collisions in the energy range 69 - 303 GeV/c for K_s production and 69 - 205 GeV/c for Λ production.[15] These data indicate that there is little or no energy dependence of the function ϕ, as predicted by the KNO scaling hypothesis. In Figure 4(b), we show the results from this experiment only. Our data from pp collisions agrees with that reported by Cohen, and this experiment shows no detectable difference in the data from different beam types at the same energy. Furthermore, there appears to be no significant difference in the data between K_s and Λ production. There is no reason to expect that the function ϕ would be the same for these two particles, since they are produced by quite different mechanisms. The K_s production occurs predominantly in the central region of rapidity space, due presumably to the combination of two "sea" quarks. However, Λ production is the result of target fragmentation, and is generally supposed to be the combination of two of the valence quarks of the proton with a sea

quark. In addition Λ production is very nearly multiplicity-independent, while K_s appears from Figure 3 to vary with multiplicity. Therefore, it is somewhat surprising that the two sets of data in Figure 4 appear to be so nearly the same.

IV. Inclusive Distributions

A. Longitudinal Variables

In analyzing the K_s production in this experiment, it is appropriate to begin with the results from the proton beam for several reasons. First, the symmetry inherent in the longitudinal direction of the initial center-of-mass system requires the distribution of any final-state particle to be symmetric about $y = 0$. Since this experiment was performed in a small bubble chamber at very high energy, this expected symmetry provides a necessary check to determine that bias in the forward direction is properly corrected using the longitudinal distributions of the neutral particles studied. In Figure 5 the weighted rapidity distribution for reaction (3) has been folded about $y = 0$ and plotted on the same scale. A χ^2 fit was performed to the weighted average of the two, and it was determined that the two halves of this distribution are the same with a χ^2 of 3.2 for 8 degrees of freedom. Therefore, we may conclude that the event weighting scheme adequately corrects for the systematic bias against the detection of neutrals with rapidity between -2 and +2.

A second reason for beginning with the K_s produced from the proton beam is that experiments with proton beams have been done at energies above and below the energy of this experiment[1-7]. Therefore, the results could be compared with those of other experiments. There

are no other data on results from K^+ production of K_s at these energies, and there has been only one π^+ beam experiment, at 100 GeV/c[1]. Some experiments have been done with a π^- beam, and comparisons will be made with these experiments when appropriate.

In Figure 6a the rapidity distribution in the backward hemisphere of K_s produced in pp collisions at 147 GeV/c (this experiment) is compared with the distribution of K_s produced in pp collisions at 300 GeV/c[6]. These plots clearly indicate that K_s production occurs in the central region of rapidity space. The shapes of these two curves are the same, and there is no indication of a central region plateau in either one. The formation of the central region plateau with increasing energy should be characterized by the broadening of the central region. This is not the case here, so it may be concluded that, at presently accessible energies, there is no indication of the central region plateau expected as a consequence of the multi-peripheral model.

The backward hemisphere Feynman x distributions of K_s production from pp collisions at different energies are presented in Figure 6b[16]. From this collection of data it may be conjectured that scaling in the Feynman x variable has begun by 150 GeV/c in pp collisions, possibly by 100 GeV/c. The scaling is approached from below; that is, as the energy of the beam increases, the height of the distribution also increases, until there is no observable change in the distribution from about 100 GeV/c to 300 GeV/c.

The rapidity distribution for K_s production from π^+ beams at 147 GeV/c is plotted in Figure 7a, along with the distribution from π^- beams at the same energy[13]. The distributions are identical,

within the experimental uncertainties, indicating that K_s production may proceed via the same mechanism in π^+p and π^-p collisions.

Figure 7b shows the Feynman x distribution for inclusive K_s production at 147 GeV/c in π^+p collisions. This plot makes it obvious that K_s production in π^+p collisions is not symmetric about $x = 0$, but has a larger cross section for $x > 0$ than for $x < 0$. This forward shift has been observed before, as indicated by the data on the same graph from an 18.5 GeV/c π^-p experiment[17].

In Figure 8 the rapidity and Feynman x distributions for K_s production from reaction (2) are shown. Although the experimental uncertainties for these distributions are larger than those for reaction (1) and (3) due to lower statistics, several observations may be made about these spectra. First, one expects a large contribution to the inclusive K_s cross section from diffractive beam dissociation events where the initial strangeness of the beam is carried through as a fast K_s. From this figure, it appears as if the beginning of the forward peak is visible; however, there are several systematic reasons for the fact that we have been unable to observe the fast K_s in this data sample. The number of K^+ beam events is small, and the very fast K_s produced will almost always decay outside the bubble chamber. A crude calculation shows that, in the data sample used, one expects to see only one or two of these fast K_s. Just one K_s in the chamber with a momentum of 120 GeV/c would add approximately 0.7 mb to the K_s cross section, increasing it by over ten per cent.

One other observation may be made about the K_s distributions. For the rapidity region $y < 1.5$ and the Feynman x region $x \leq 0.2$,

the K_s spectra from the K^+ beam match those from the π^+ beam. The heights of the plots at x = 0 and y = 0 are the same, and they fall off from zero at the same rate. This implies that the production of central region K_s is the same for π^+p and π^-p collisions as it is for K^+p collisions.

One expects the inclusive production of Λ to occur mainly in the target fragmentation region, and this is seen in plots of Feynman x in Figure 9 for reactions (4) - (6). It is evident that there is a peak in inclusive production at x ~ -0.5 or -0.6 for all three types of beams. Furthermore, there is some central region production of Λ and the height of the Feynman x distribution at x = 0 is approximately one-half of that of the backward peak in all three beam types. In fact, the three plots are similar to one another, and, within experimental errors, the shapes appear to be consistent with one another, apart from the overall normalization.

The production of Λ from the proton beam should be symmetric about x = 0, but we observe that this is true only out to about x = 0.4. This is another result of the systematic bias against detection of fast-forward neutral particles. The backward hemisphere distribution of Feynman x for pp collisions at different energies is shown in Figure 10[16]. From this figure, it is evident that Feynman scaling in inclusive Λ production by protons has been achieved by a lab momentum of at most 100 GeV/c.

In Figure 11, the backward hemisphere rapidity distribution for Λ produced from proton beams in this experiment is compared with that at 300 GeV/c[6]. From this plot it is difficult to determine whether the rapidity distribution is expanding with energy. With the notable exception of the point at lowest rapidity, the

points at the two energies are consistent with one another. One does not expect much variation with beam energy of the Λ produced from target fragmentation. However, the peak of this component should move farther from $y = 0$ as energy increases, and the centrally produced Λ should expand with increased energy. The data presented in the figure are inconclusive, and resolution of this matter depends on either higher statistics experiments or future experiments at higher energies.

Rapidity distributions for reactions (4) and (5) are shown in Figure 12, along with that from the π^- experiment done at the same energy[13]. The two pion experiments are consistent with one another, within experimental errors. As with the centrally-produced K_s, the target-fragmentation and central Λ produced by meson beams are quite similar.

The $\bar{\Lambda}$ rapidity distributions for this experiment are shown in Figure 13a, and the Feynman x distributions are shown in Figure 13b. From these plots, it is evident that $\bar{\Lambda}$ production takes place in the central region. The heights of the plots at $y = 0$ and at $x = 0$ are consistent with being the same for the two meson beams, as well as being consistent with that from the π^- experiment at the same energy. The same result was observed in K_s production, which also occurs in the central region. The cross sections for both K_s and $\bar{\Lambda}$ production are rising at these energies, and there is no evidence in either case for a central region plateau.

It is interesting to note that the values of $d\sigma/dy$ at $y = 0$ for Λ° are consistently higher for each beam than the corresponding values for $\bar{\Lambda}$. This indicates that central region Λ production is not solely the result of $\Lambda\bar{\Lambda}$ production. It may be that some of the

central region Λ are the result of a "tail" of target fragmentation production.

B. Transverse Momentum

In examining the transverse momentum spectra for inclusive K_s production, it is again appropriate to begin with the results from the pp collisions. In Figure 14 the square of the transverse momentum is plotted for K_s production from this experiment as well as other experiments done at different energies with proton beams[16]. The distributions are integrated over longitudinal space, and the plot is logarithmic in the vertical scale. It appears as if the plots of $d\sigma/dp_t^2$ for energies higher than 100 GeV are indistinguishable out to approximately 1.0 GeV^2/c^2. It is evident that the data at all energies can be well-fit by the functional form $Ae^{-bp_t^2}$. The value for b of 4.0 ± 0.9 $(GeV/c)^{-2}$ for the data from this experiment agrees well with the values of 3.2 ± 1.4 $(GeV/c)^{-2}$ and 4.6 ± 0.8 $(GeV/c)^{-2}$ for 205 GeV/c pp collisions[3,16] and a value of approximately 4.3 ± 0.7 $(GeV/c)^{-2}$ derived from the 300 GeV/c experiment[6].

The transverse momentum spectra for K_s production from all three beams in this experiment are shown in Figure 15, along with the fits to the form $Ae^{-bp_t^2}$. Note that, although the value for b for K_s production from K^+ beams is somewhat higher than the other two, all three values are in agreement within the experiment uncertainties. For completeness, the Lorentz-invariant distributions of transverse momentum squared are shown in Figure 16. The data for pp collisions at 205 GeV/c and 300 GeV/c are also plotted here[6], and the same apparent scaling reported above is also evident here.

In Figures 17 and 18 are shown the p_t^2 distributions for Λ and $\bar{\Lambda}$ respectively, for all three beam particles from this experiment. Although the data in the figures are consistent with being exponential in shape, the values for b for both Λ and $\bar{\Lambda}$ production appear to vary with beam type in this experiment. In fact, when comparing the data from π^+ and p beams (K^+ beam data are too scarce to warrant comparison), the Λ and $\bar{\Lambda}$ data have consistent slopes within beam types; however, the slopes for the π^+ beam are different from those for the p beam. Table VI summarizes the fitted slopes from various experiments by beam type. From this table, it is evident that the slopes of $\Lambda/\bar{\Lambda}$ production from the π^+ beam in this experiment are somewhat higher than those from π^- beams at higher energies. It is interesting to note that the two lower energy points from π^- beams are also conssitent with having larger slopes than the higher energy data.

This work was supported in part by the U.S. Department of Energy and the National Science Foundation. We gratefully acknowledge the efforts of the 30-inch bubble chamber crew and the scanning and measuring personnel at the participating institutions.

References

1. M. Alston-Garnjost et al., Phys. Rev. Lett. 35, 142 (1975).
2. J. Chapman et al., Phys. Lett. 47B, 465 (1973).
3. G. Charlton et al., Phys. Rev. Lett. 30, 574 (1973).
4. K. Jaeger et al., Phys. Rev. D11, 2405 (1975).
5. F. Dao et al., Phys. Rev. Lett. 30, 1151 (1973).
6. A. Sheng et al., Phys. Rev. D11, 1733 (1975).
7. H. Kichini et al., Phys. Lett. 72B, 411 (1978).
8. D. Fong et al., Phys. Lett. 53B, 290 (1974).
9. D. Fong et al., Nucl. Phys. B102, 386 (1976).
10. D. Brick et al., Proceedings of the XIX International Conference on High Energy Physics, Tokyo, Japan, Aug. 1978, to be published.
11. Data other than this experiment are taken from J. Whitmore, Physics Reports 27C, 187 (1976).
12. R. D. Field and R. P. Feynman, Nucl. Phys. B136, 1 (1978).
13. "Neutral Particle Production in $\pi^- p$ Interactions at 147 GeV/c and Comparison to Charged Particle Production", Proportional Hybrid Spectrometer Consortium, to be submitted to Physical Review.
14. F. T. Dao and J. Whitmore, Phys. Lett. 46B, 252 (1973).
15. D. Cohen, Phys. Lett. 47B, 457 (1973).
16. Data other than this experiment are taken from J. Whitmore, Physics Reports 10C, 273 (1974).
17. P. H. Stuntebeck et al., Phys. Rev. D9, 608 (1974).
18. D. Ljung et al., Phys. Rev. D15, 3163 (1977).
19. D. Bogert et al., Phys. Rev. D16, 2098 (1977).

TABLE I: Events By Beam Type

Beam	Total No. of Events	Cross Section Equivalent (μb/event)
π^+	8479	2.34
K^+	1200	14.13
p	8365	3.78

TABLE II: Final Data Sample By Fit Type

Unambiguous Fits		Ambiguous Fits	
K	870	$K\Lambda$	208
Λ	308	$K\bar{\Lambda}$	98
$\bar{\Lambda}$	24	$K\gamma$	81
γ	1774	$\Lambda\gamma$	133
		$\bar{\Lambda}\gamma$	122

TABLE III: Total Inclusive Cross Sections

Reaction	Inclusive Cross Section (in mb)
$\pi^+ p \rightarrow K_s$ + anything	4.0 ± 0.3
$K^+ p \rightarrow K_s$ + anything	5.9 ± 1.0
$pp \rightarrow K_s$ + anything	5.0 ± 0.2
$\pi^+ p \rightarrow \Lambda$ + anything	1.8 ± 0.2
$K^+ p \rightarrow \Lambda$ + anything	1.4 ± 0.4
$pp \rightarrow \Lambda$ + anything	4.2 ± 0.2
$\pi^+ p \rightarrow \bar{\Lambda}$ + anything	0.7 ± 0.1
$K^+ p \rightarrow \bar{\Lambda}$ + anything	0.5 ± 0.2
$pp \rightarrow \bar{\Lambda}$ + anything	0.8 ± 0.2

TABLE IV: Topological Cross Sections for K_s^o Production

	σ_n (in mb)		
	BEAM		
Multiplicity	π^+	K^+ †	p
2	0.16±0.06	0.04±0.04	0.30±0.07
4	0.68±0.18	0.92±0.34	0.66±0.11
6	0.85±0.15	0.56±0.18	1.28±0.19
8	0.92±0.12	0.54±0.17	0.96±0.12
10	0.72±0.09	0.88±0.27	0.63±0.10
12	0.45±0.07	0.41±0.15	0.55±0.09
14	0.24±0.07	0.04±0.04	0.12±0.04
16	0.02±0.02	0.05±0.05	0.06±0.03
18	0.04±0.02	—	0.01±0.01
20	0.01±0.01	0.06±0.06	0.02±0.02

† In the K^+ beam sample, K_s^o events with rapidity > 1.5 have been eliminated.

TABLE V: Topological Cross Sections for Λ Production

(backward hemisphere only)

Multiplicity	σ_n (in mb) BEAM	
	π^+	p
2	0.11 ± 0.04	0.18 ± 0.05
4	0.15 ± 0.04	0.44 ± 0.07
6	0.27 ± 0.05	0.41 ± 0.08
8	0.34 ± 0.06	0.52 ± 0.09
10	0.14 ± 0.03	0.31 ± 0.07
12	0.10 ± 0.03	0.13 ± 0.05
14	0.03 ± 0.02	0.08 ± 0.03
16	0.04 ± 0.02	0.04 ± 0.02
18	0.01 ± 0.01	———

TABLE VI: Transverse Momentum Squared Slopes for Λ and $\bar{\Lambda}$ Production

Beam Lab Momentum	Beam Type	Slope $(GeV/c)^{-2}$	
21-28 GeV/c[3]	p	Λ^o: 3.6±0.4	
40 GeV/c[18]	π^-	Λ^o: 4.7±0.9	
147 GeV/c	π^+	Λ^o: 4.2±0.1	$\bar{\Lambda}^o$: 4.2±0.1
	p	Λ^o: 2.9±0.7	$\bar{\Lambda}^o$: 3.2±0.1
205 GeV/c[18]	π^-	Λ^o: 3.2±0.1	$\bar{\Lambda}^o$: 3.8±1.3
	p	Λ^o: 2.7±0.7	
250 GeV/c[19]	π^-	Λ^o: 3.0±0.3	$\bar{\Lambda}^o$: 2.5±0.6
400 GeV/c[7]	p	Λ^o: 3.3±0.4	$\bar{\Lambda}^o$: 3.7±1.3

Figures

1. Center-of-mass decay angle distributions for final samples of (a) K_s, and (b) Λ.
2. Total inclusive cross sections as a function of incident beam lab momentum for (a) K_s, (b) Λ, and (c) $\bar{\Lambda}$.
3. $\langle V^o \rangle_n$ vs. multiplicity for (a) K_s and (b) Λ by beam types.
4. KNO scaling plots for K_s and Λ. The curves are Cohen's fits to pp data. (a) KNO plot for K_s from several pp experiments. (b) KNO plot for K_s from this experiment only, for all three beams. (c) KNO plot for Λ from several pp and π^+p experiments.
5. Rapidity distribution, folded about $y = 0$, for K_s produced in pp collisions in this experiment.
6. (a) Backward hemisphere rapidity distribution of K_s produced in pp collisions at 147 GeV/c and 300 GeV/c.

   (b) Backward hemisphere Feynman x distributions of K_s produced in pp collisions at various energies.
7. (a) Rapidity distributions of K_s produced at 147 GeV/c from π^+ and π^- beams.

   (b) Feynman x distribution of K_s from π^+ beams in this experiment compared to π^- beam at 18.5 GeV/c.
8. (a) Rapidity distribution of K_s from K^+ beams in this experiment.

   (b) Feynman x distribution of K_s from K^+ beams in this experiment.
9. Feynman x distribution of Λ by beam type.
10. Backward hemisphere Feynman x distribution of Λ production in pp collisions at various energies.
11. Backward hemisphere rapidity distribution of Λ from pp collisions at 147 GeV/c and 300 GeV/c.

12. Rapidity distributions of Λ from π^+, π^-, and K^+ beams at 147 GeV/c.

13. (a) Rapidity distributions of $\bar{\Lambda}$ from this experiment by beam type.

    (b) Feynman x distributions of $\bar{\Lambda}$ from this experiment by beam type.

14. Transverse momentum squared distribution for K_s from pp collisions at various energies.

15. Transverse momentum squared distribution for K_s from this experiment by beam type.

16. Lorentz-invariant transverse momentum squared distribution for this experiment by beam type and for pp collisions at 205 GeV/c and 300 GeV/c.

17. Transverse momentum squared distribution for Λ from this experiment by beam type.

18. Transverse momentum squared distribution for $\bar{\Lambda}$ from this experiment by beam type.

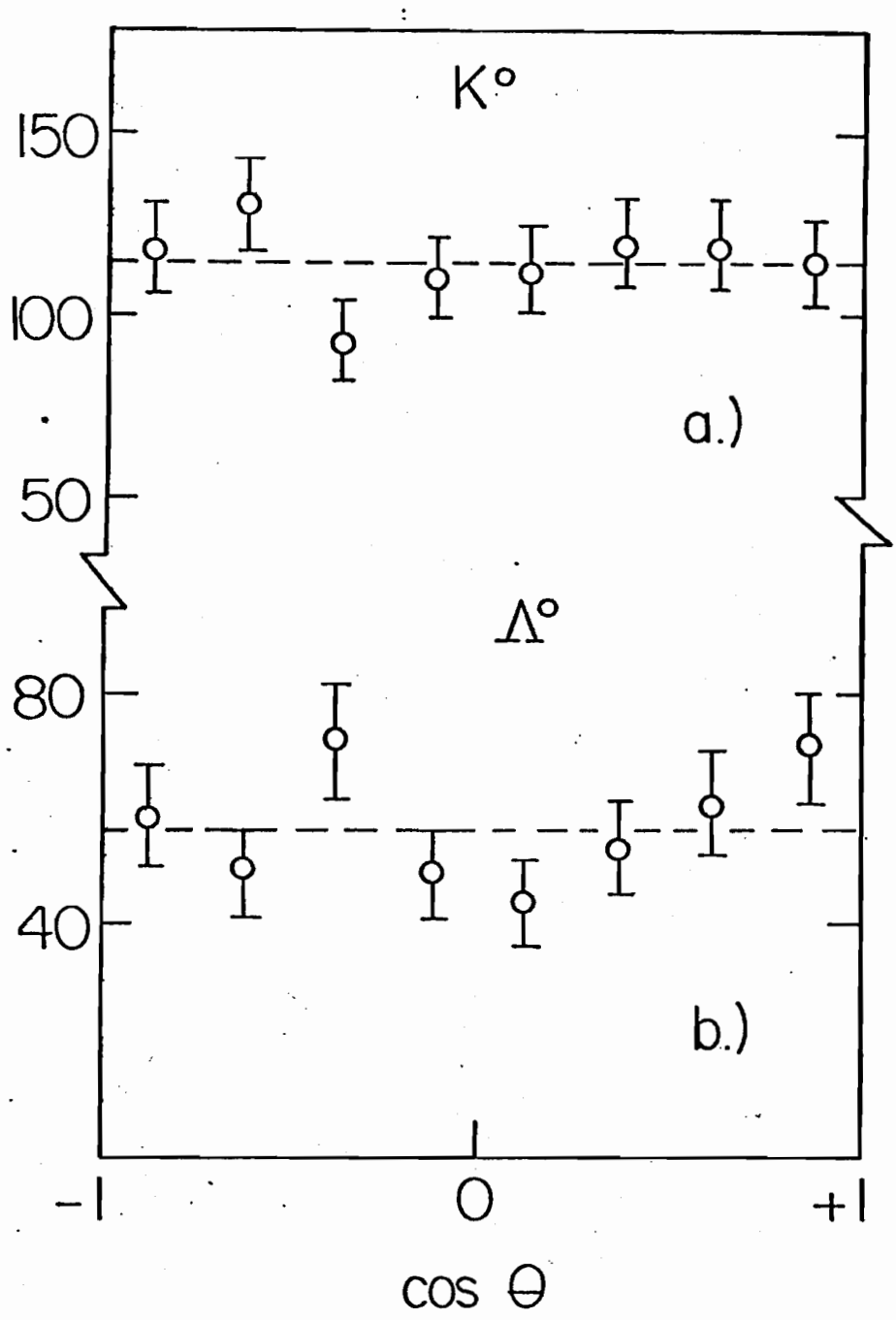

FIG. 1

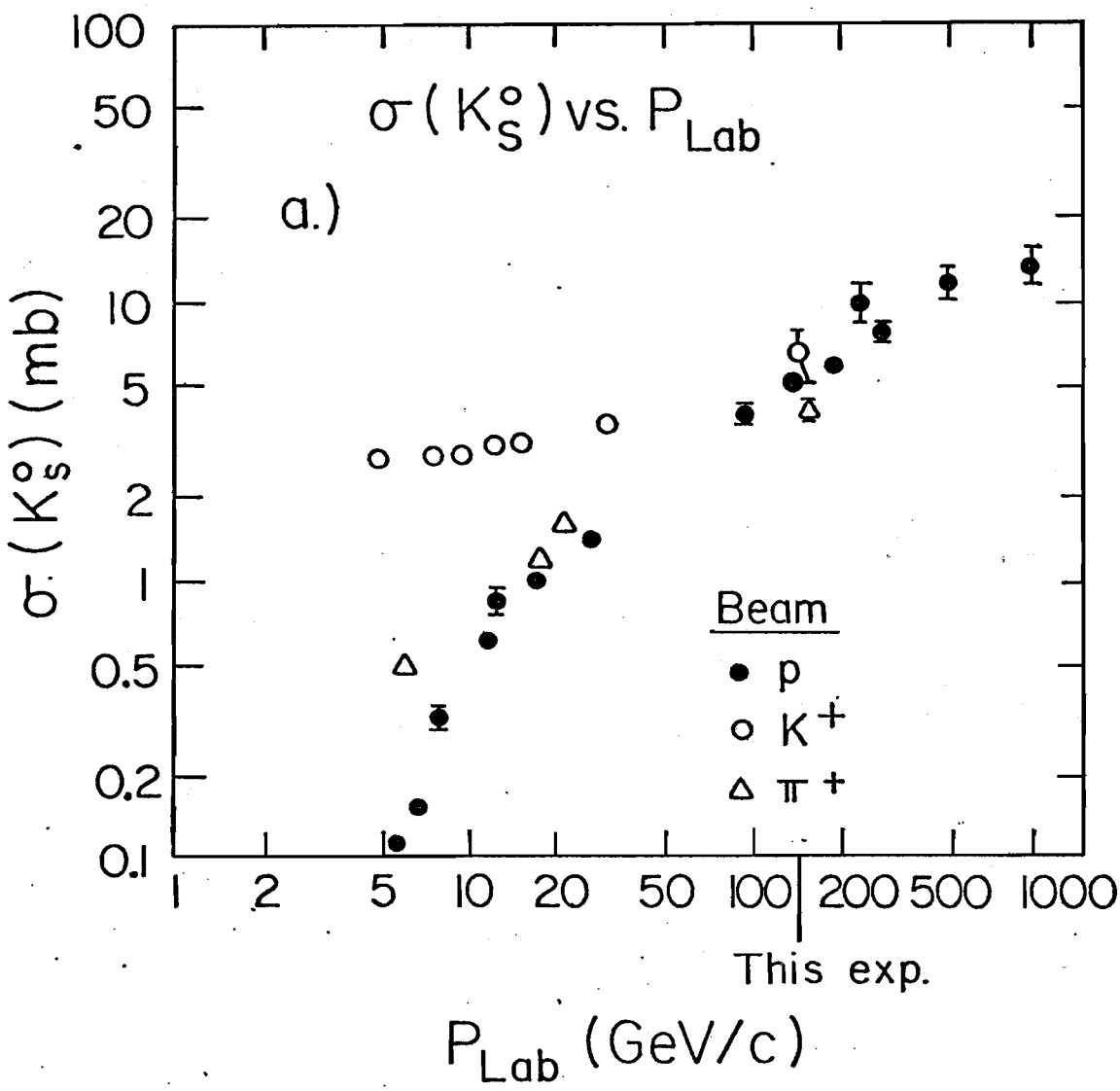
σ(K°S) vs. PLab
a.)
σ(K°S) (mb)
100
50
20
10
5
2
1
0.5
0.2
0.1
1
2
5
10
20
50
100
200
500
1000
This exp.
PLab (GeV/c)
Beam
p
K+
π+

FIG. 2 a)

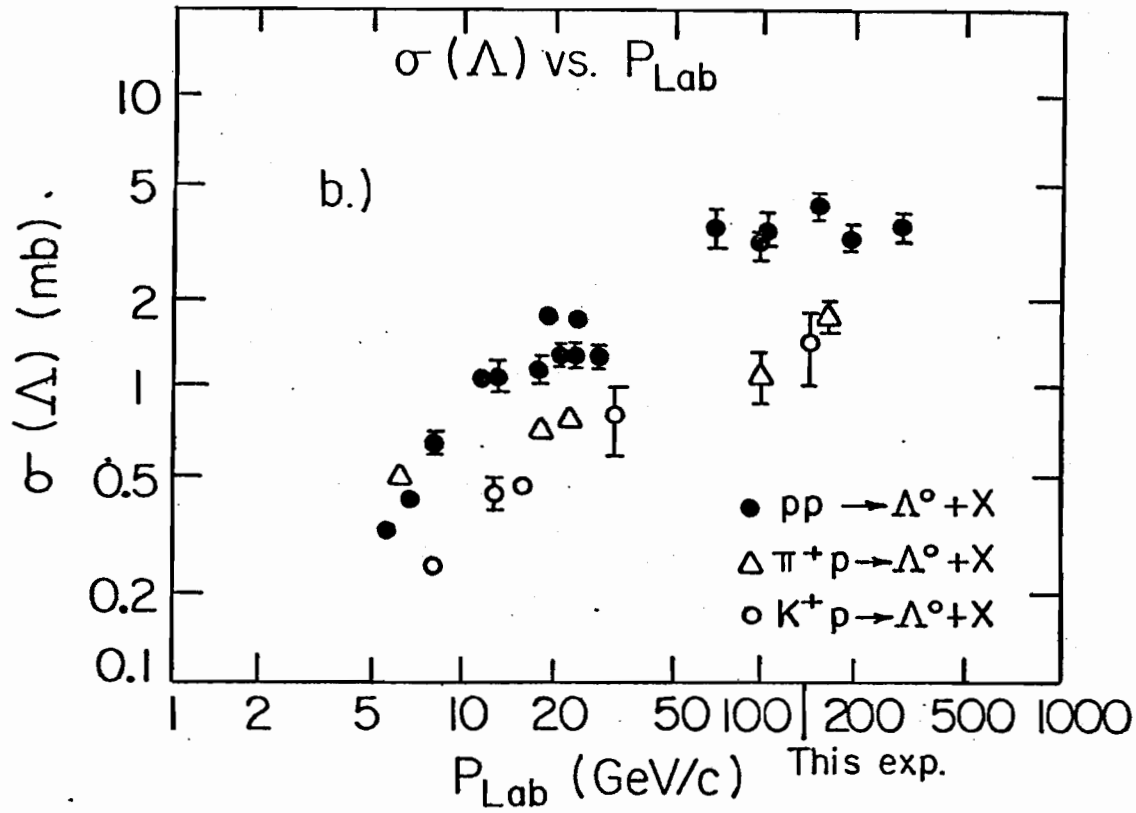
σ (Λ) vs. P_Lab
b.)
σ (Λ) (mb)
10
5
2
1
0.5
0.2
0.1
● pp → Λ° + X
△ π⁺p → Λ° + X
○ K⁺p → Λ° + X
1
2
5
10
20
50
100
200
500
1000
P_Lab (GeV/c)
This exp.

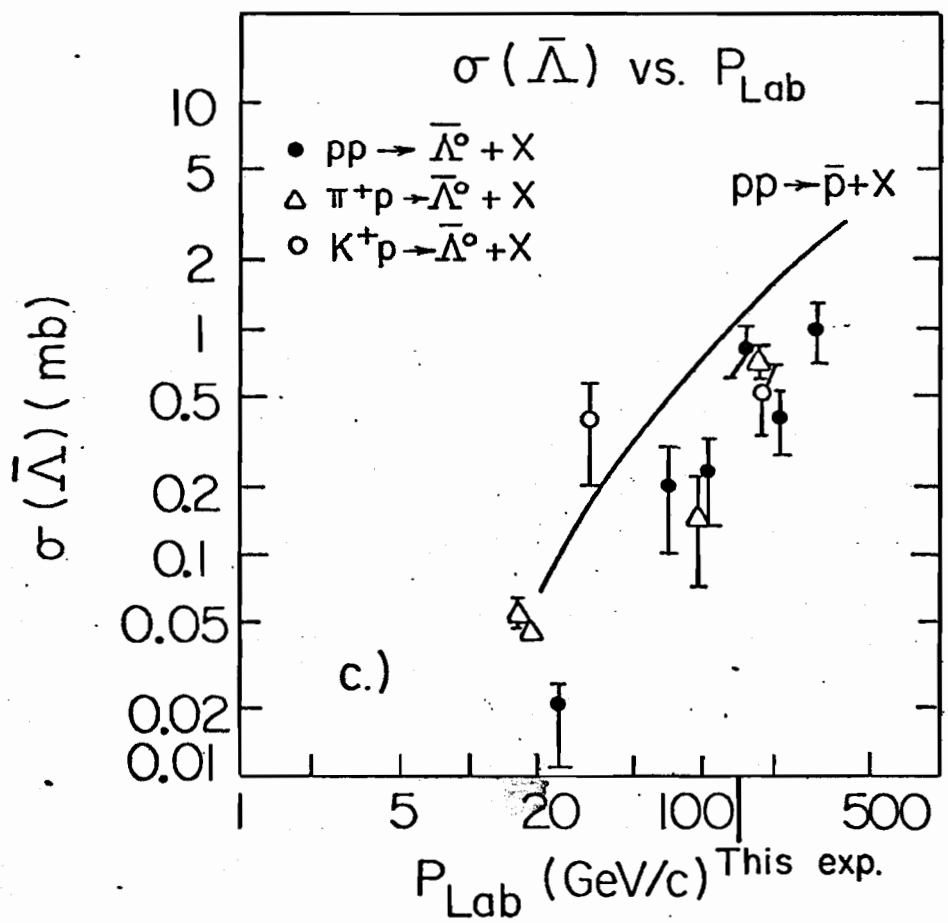
σ (Λ̄) vs. P_Lab
● pp → Λ̄° + X
△ π⁺p → Λ̄° + X
○ K⁺p → Λ̄° + X
pp → p̄ + X
c.)
σ (Λ̄) (mb)
10
5
2
1
0.5
0.2
0.1
0.05
0.02
0.01
1
5
20
100
500
P_Lab (GeV/c)
This exp.

Fig. 2 (b), (c)

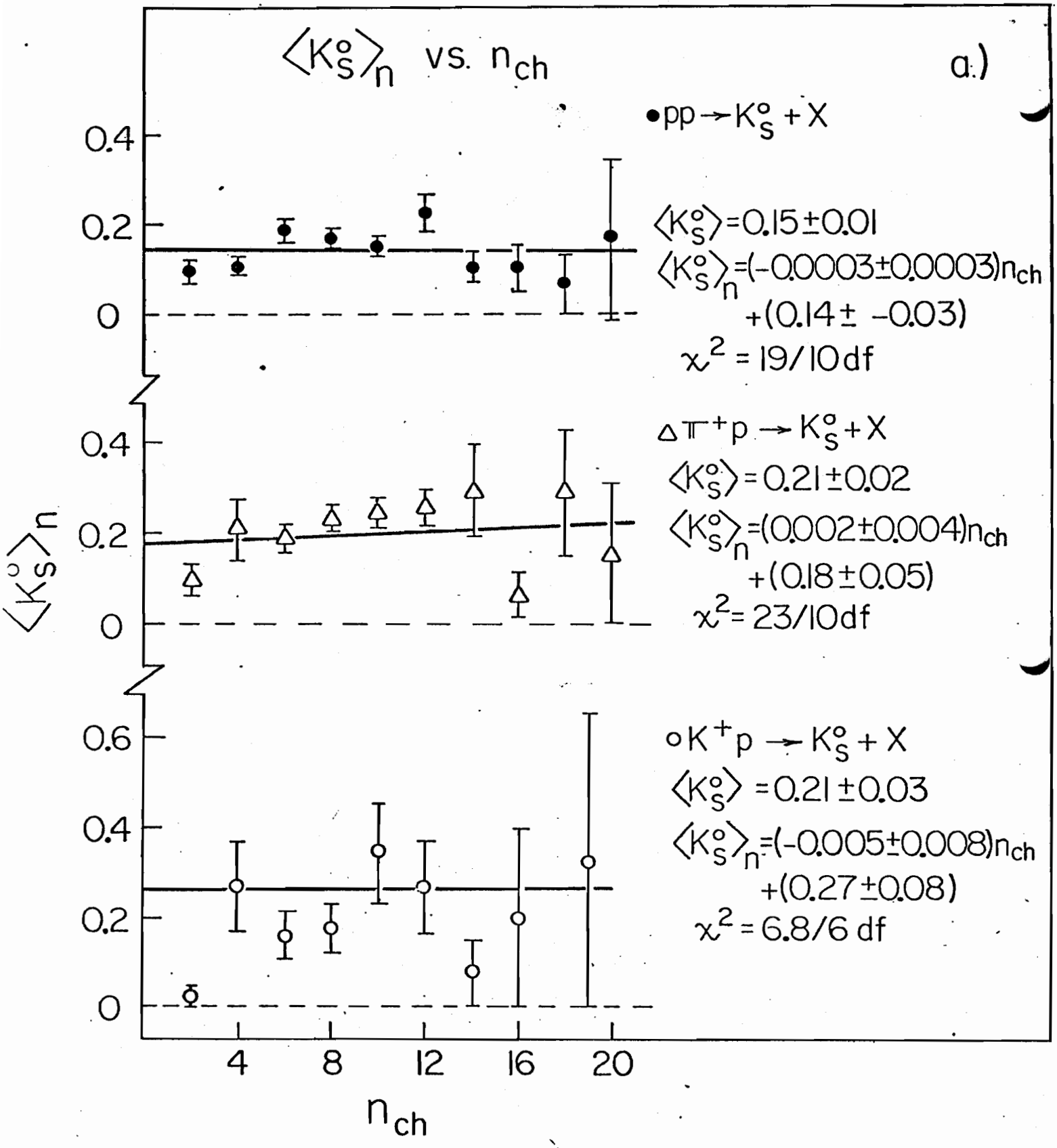
$\langle K_s^o \rangle_n$ vs. n_{ch}
a.)
• $pp \to K_s^o + X$
$\langle K_s^o \rangle = 0.15 \pm 0.01$
$\langle K_s^o \rangle_n = (-0.0003 \pm 0.0003) n_{ch} + (0.14 \pm -0.03)$
$\chi^2 = 19/10$ df
$\Delta \pi^+ p \to K_s^o + X$
$\langle K_s^o \rangle = 0.21 \pm 0.02$
$\langle K_s^o \rangle_n = (0.002 \pm 0.004) n_{ch} + (0.18 \pm 0.05)$
$\chi^2 = 23/10$ df
$\circ K^+ p \to K_s^o + X$
$\langle K_s^o \rangle = 0.21 \pm 0.03$
$\langle K_s^o \rangle_n = (-0.005 \pm 0.008) n_{ch} + (0.27 \pm 0.08)$
$\chi^2 = 6.8/6$ df
$\langle K_s^o \rangle_n$
n_{ch}
0.4
0.2
0
0.6
4
8
12
16
20

FIG. 3 (a)

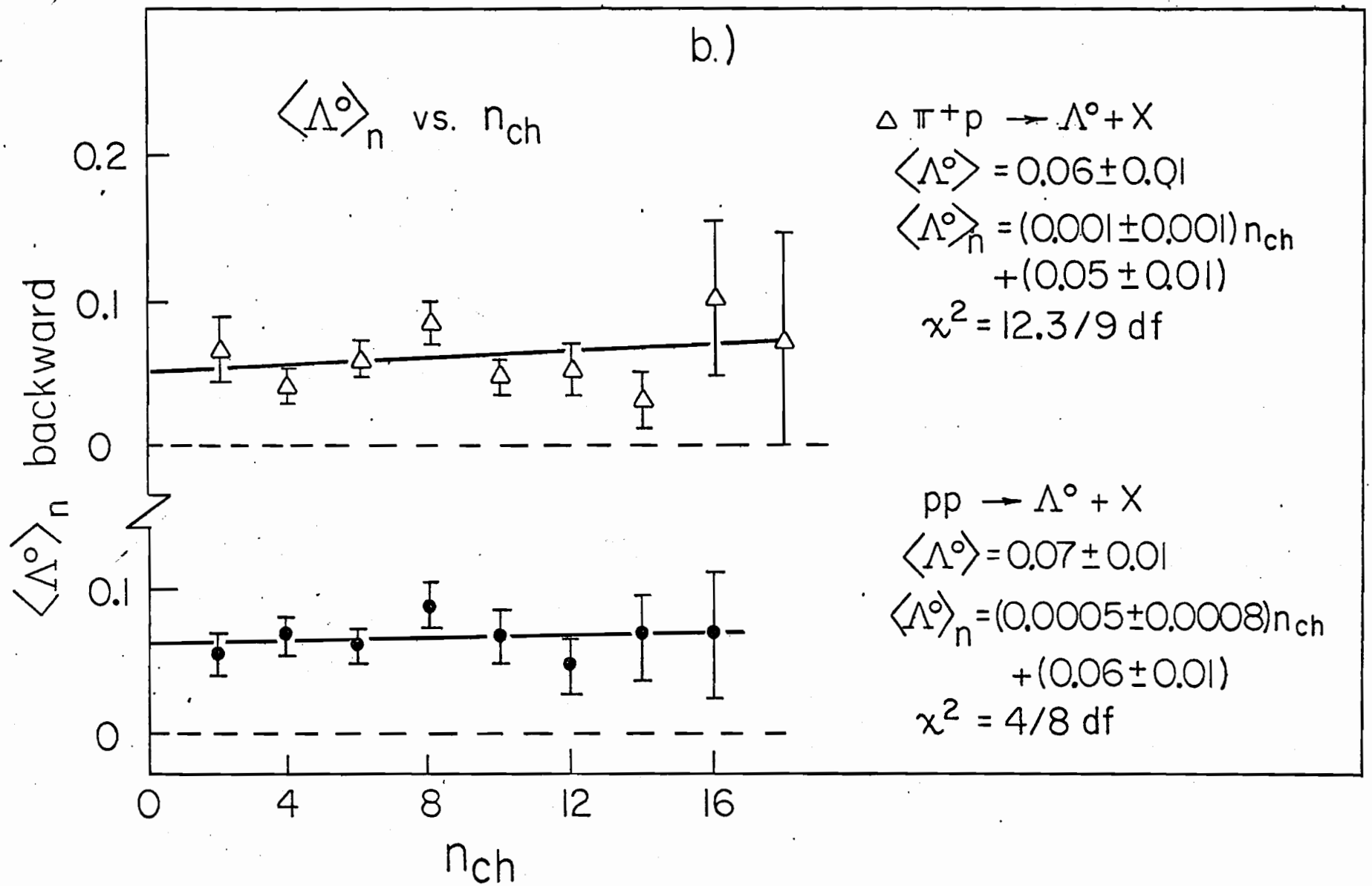
b.)
$\langle \Lambda^\circ \rangle_n$ vs. n_{ch}
$\Delta\ \pi^+ p \rightarrow \Lambda^\circ + X$
$\langle \Lambda^\circ \rangle = 0.06 \pm 0.01$
$\langle \Lambda^\circ \rangle_n = (0.001 \pm 0.001)\, n_{ch} + (0.05 \pm 0.01)$
$\chi^2 = 12.3/9$ df
$pp \rightarrow \Lambda^\circ + X$
$\langle \Lambda^\circ \rangle = 0.07 \pm 0.01$
$\langle \Lambda^\circ \rangle_n = (0.0005 \pm 0.0008)\, n_{ch} + (0.06 \pm 0.01)$
$\chi^2 = 4/8$ df
$\langle \Lambda^\circ \rangle_n$ backward
0.2
0.1
0
0.1
0
0
4
8
12
16
n_{ch}

Fig. 3 (b)

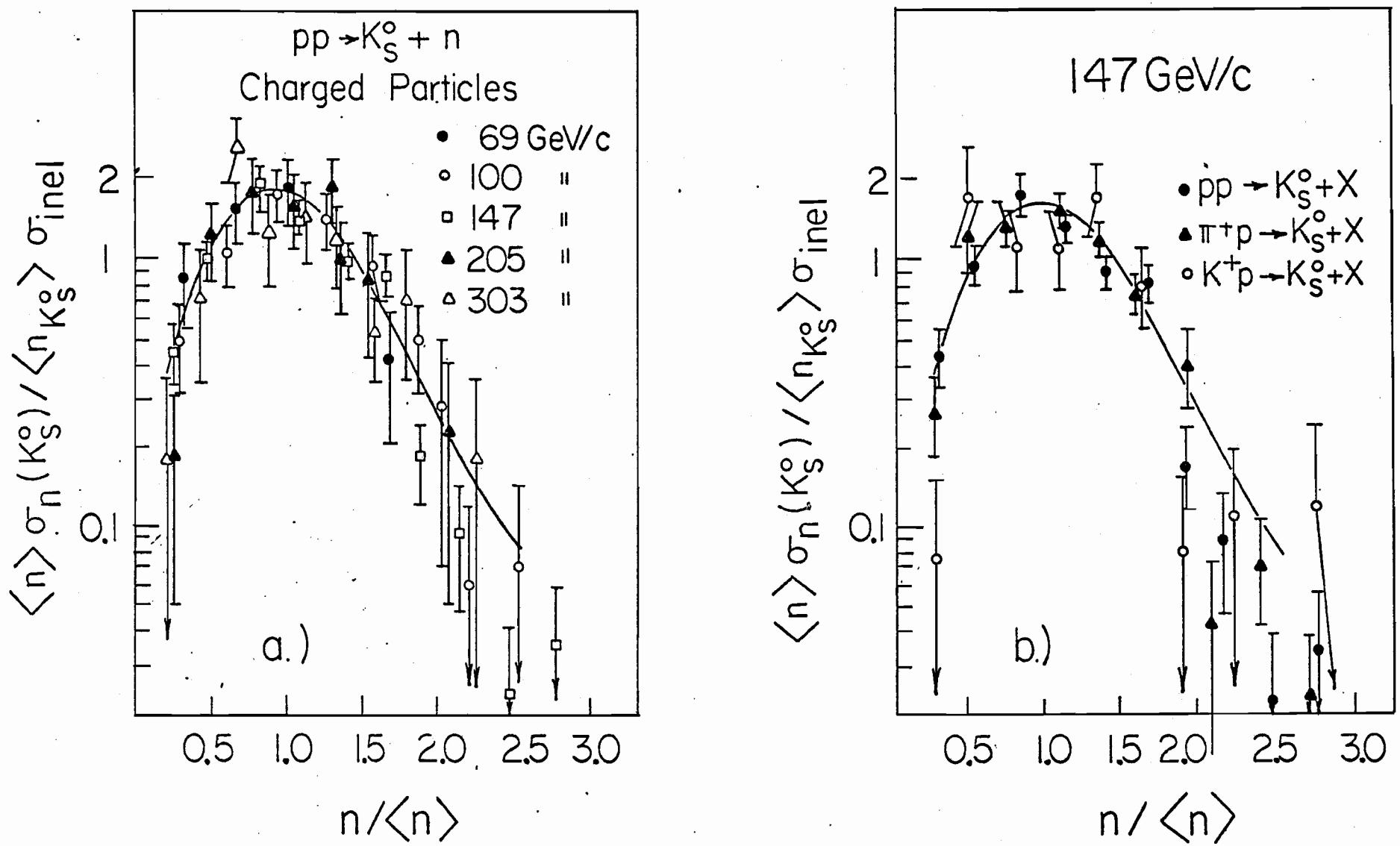
pp → K^o_S + n
Charged Particles
69 GeV/c
100 "
147 "
205 "
303 "
a.)
$\langle n \rangle \sigma_n(K^o_S) / \langle n_{K^o_S} \rangle \sigma_{inel}$
n/⟨n⟩
147 GeV/c
pp → K^o_S+X
π^+p → K^o_S+X
K^+p → K^o_S+X
b.)
$\langle n \rangle \sigma_n(K^o_S) / \langle n_{K^o_S} \rangle \sigma_{inel}$
n/⟨n⟩

FIG. 4 a), b)

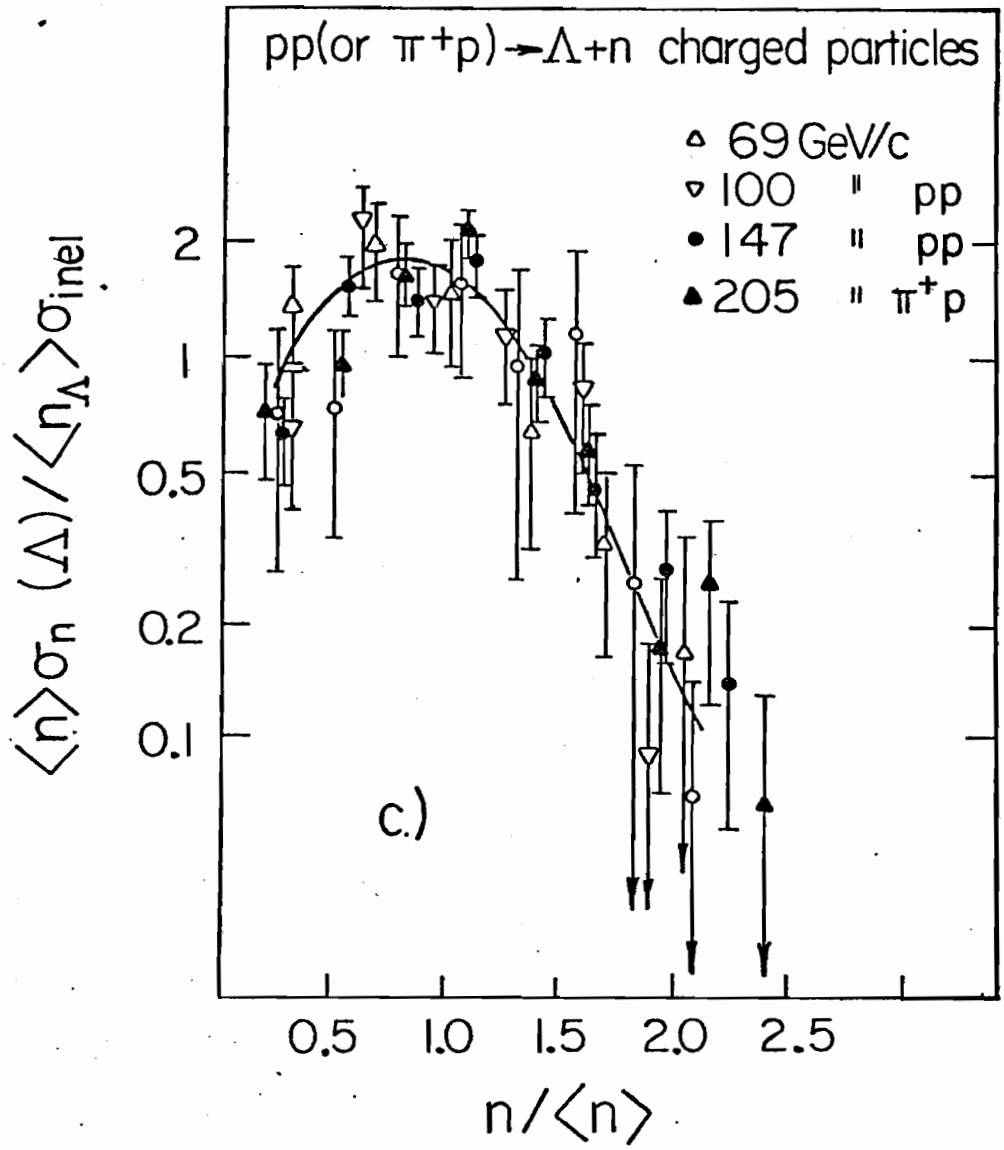
pp(or π⁺p)→Λ+n charged particles
69 GeV/c
100 " pp
147 " pp
205 " π⁺p
c.)
⟨n⟩σn (Λ)/⟨nΛ⟩σinel
2
1
0.5
0.2
0.1
0.5
1.0
1.5
2.0
2.5
n/⟨n⟩

FIG. 4 c)

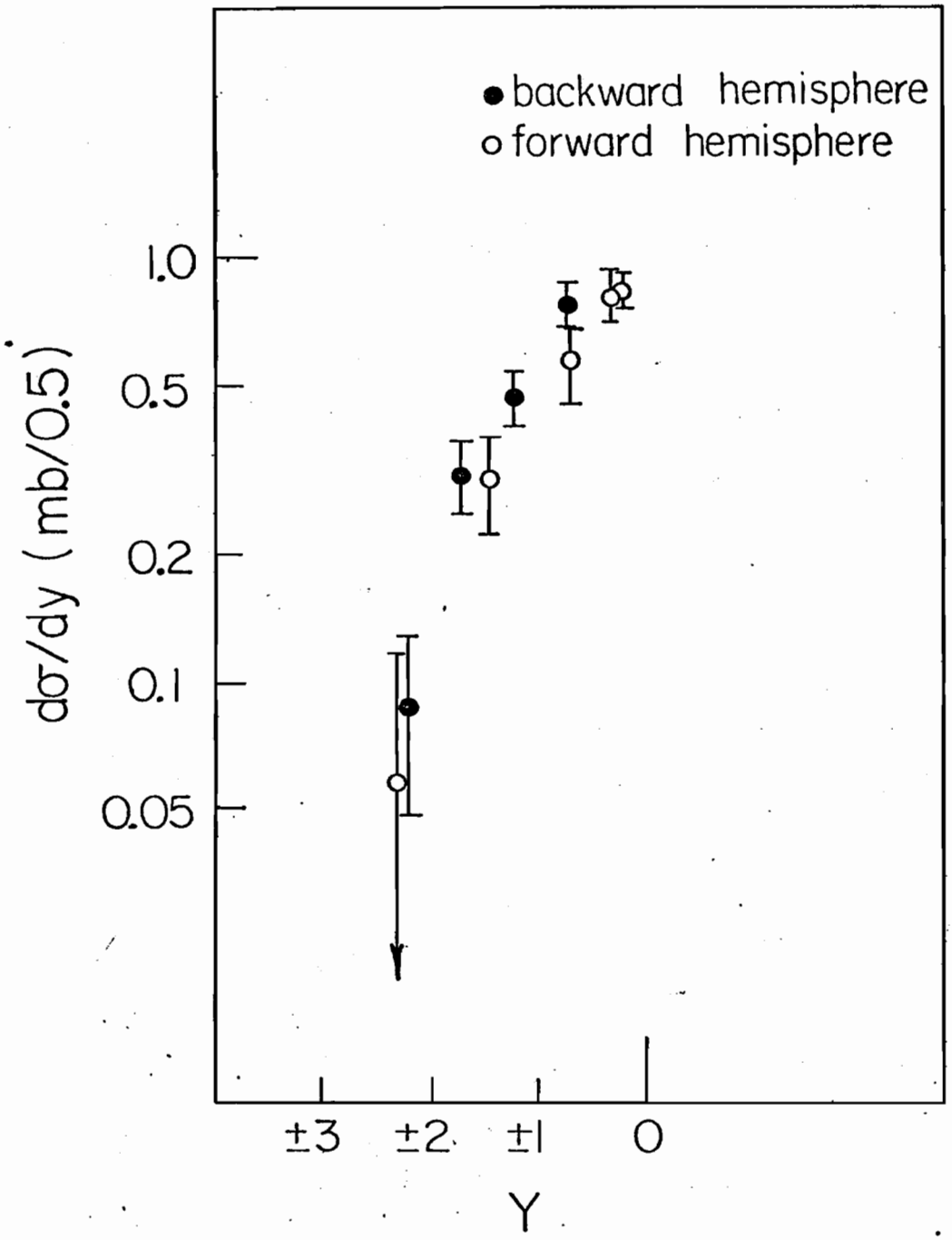
● backward hemisphere
○ forward hemisphere
1.0
0.5
0.2
0.1
0.05
dσ/dy (mb/0.5)
±3
±2
±1
0
Y

FIG. 5

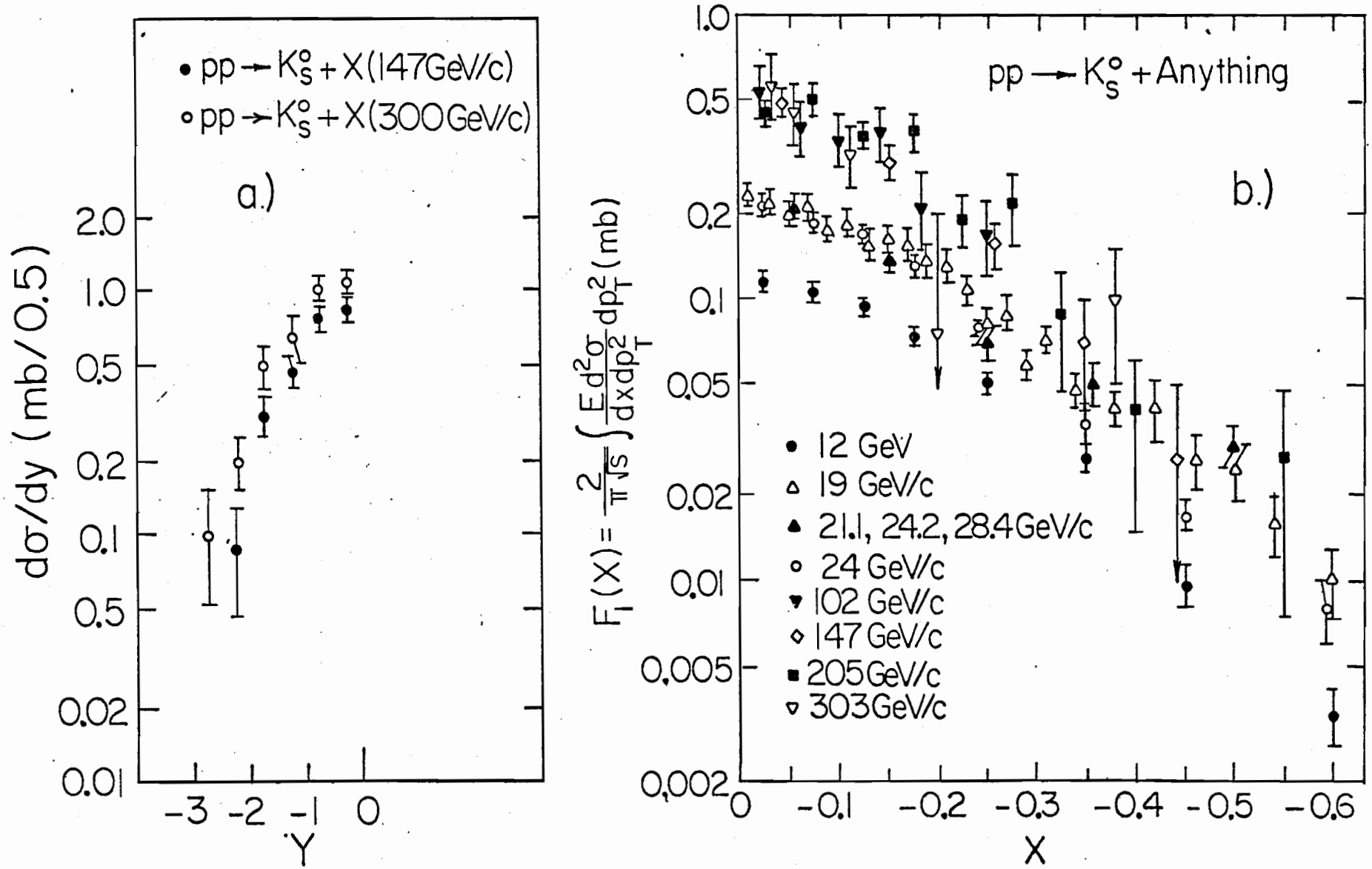
• pp → K^0_S + X(147GeV/c)
∘ pp → K^0_S + X(300GeV/c)
a.)
dσ/dy (mb/0.5)
2.0
1.0
0.5
0.2
0.1
0.5
0.02
0.01
-3 -2 -1 0
Y
pp → K^0_S + Anything
b.)
$F_1(X) = \frac{2}{\pi\sqrt{s}} \int \frac{E\,d^2\sigma}{dx\,dp_T^2} dp_T^2$ (mb)
1.0
0.5
0.2
0.1
0.05
0.02
0.01
0.005
0.002
0 -0.1 -0.2 -0.3 -0.4 -0.5 -0.6
X
• 12 GeV
△ 19 GeV/c
▲ 21.1, 24.2, 28.4 GeV/c
∘ 24 GeV/c
▼ 102 GeV/c
◇ 147 GeV/c
■ 205 GeV/c
▽ 303 GeV/c

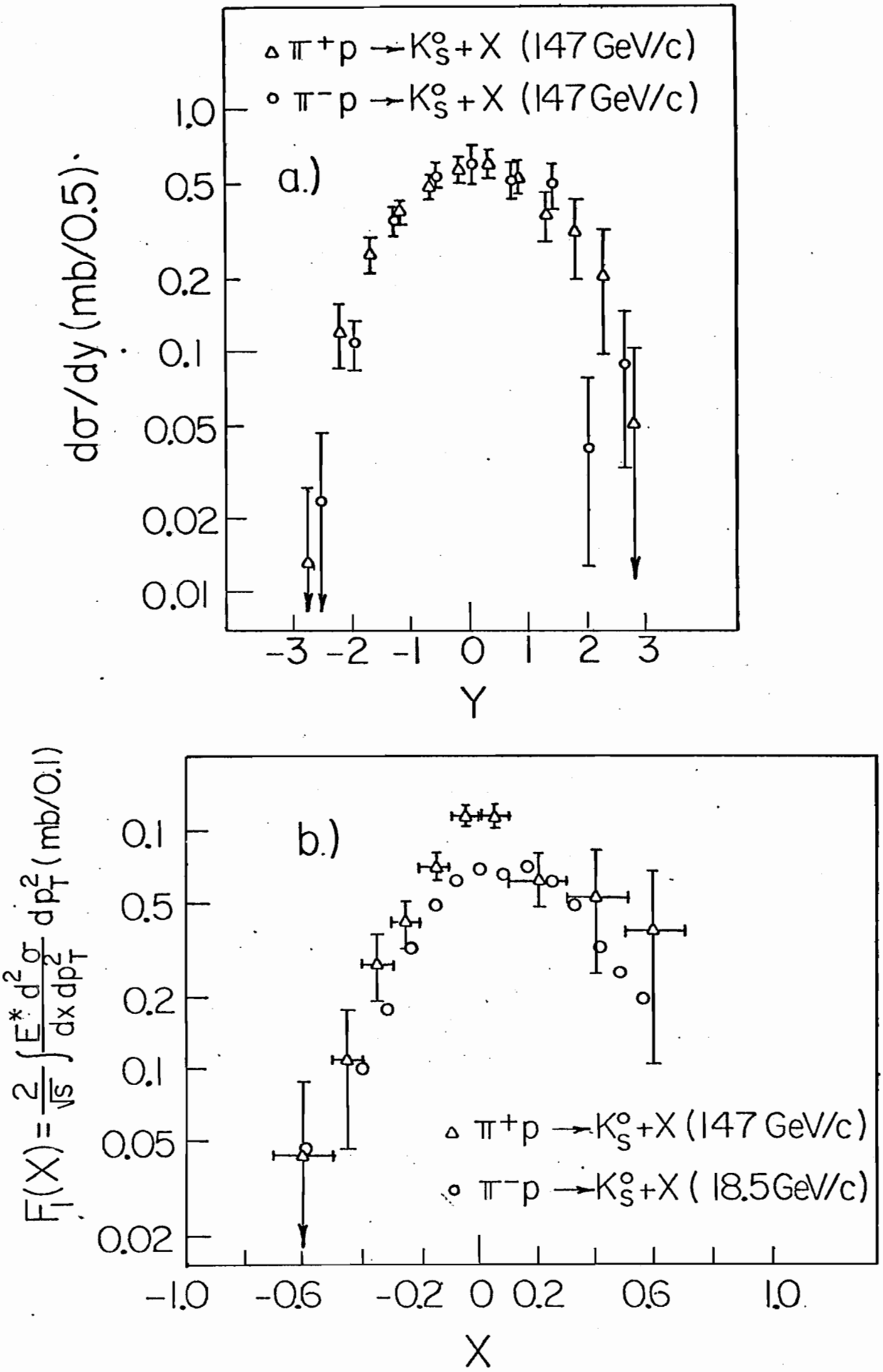
△ π⁺p → K°S + X (147 GeV/c)
○ π⁻p → K°S + X (147 GeV/c)
a.)
dσ/dy (mb/0.5)
1.0
0.5
0.2
0.1
0.05
0.02
0.01
-3 -2 -1 0 1 2 3
Y
b.)
F_I(X) = 2/√s ∫ E* d²σ/dx dp_T² dp_T² (mb/0.1)
0.1
0.5
0.2
0.1
0.05
0.02
△ π⁺p → K°S + X (147 GeV/c)
○ π⁻p → K°S + X (18.5 GeV/c)
-1.0 -0.6 -0.2 0 0.2 0.6 1.0
X

FIG. 7

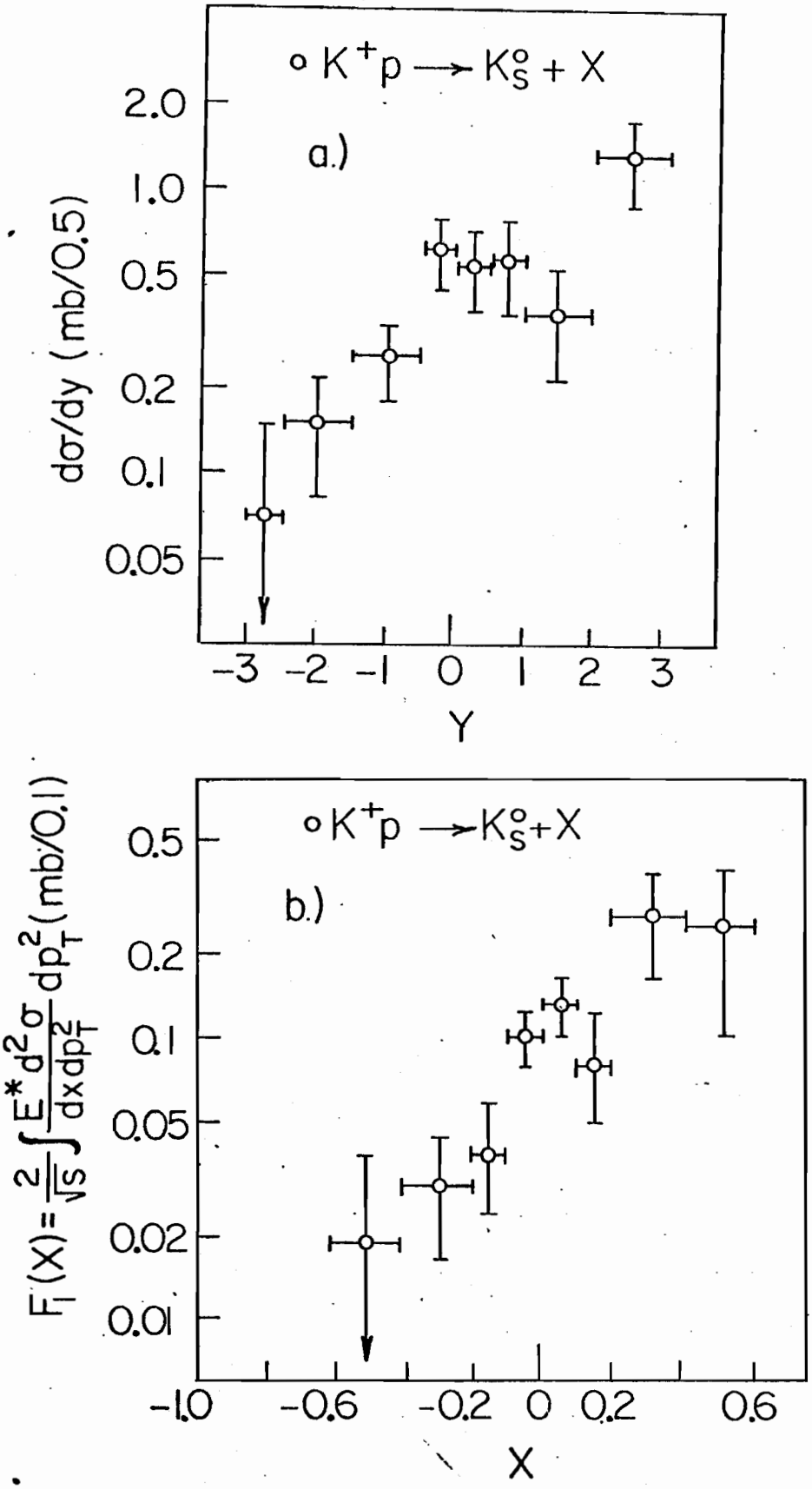
o K+p → Ks° + X
a.)
dσ/dy (mb/0.5)
2.0
1.0
0.5
0.2
0.1
0.05
-3 -2 -1 0 1 2 3
Y
o K+p → Ks°+X
b.)
F1(X) = 2/√s ∫ E* d²σ/dx dp_T² dp_T² (mb/0.1)
0.5
0.2
0.1
0.05
0.02
0.01
-1.0 -0.6 -0.2 0 0.2 0.6
X

FIG. 8

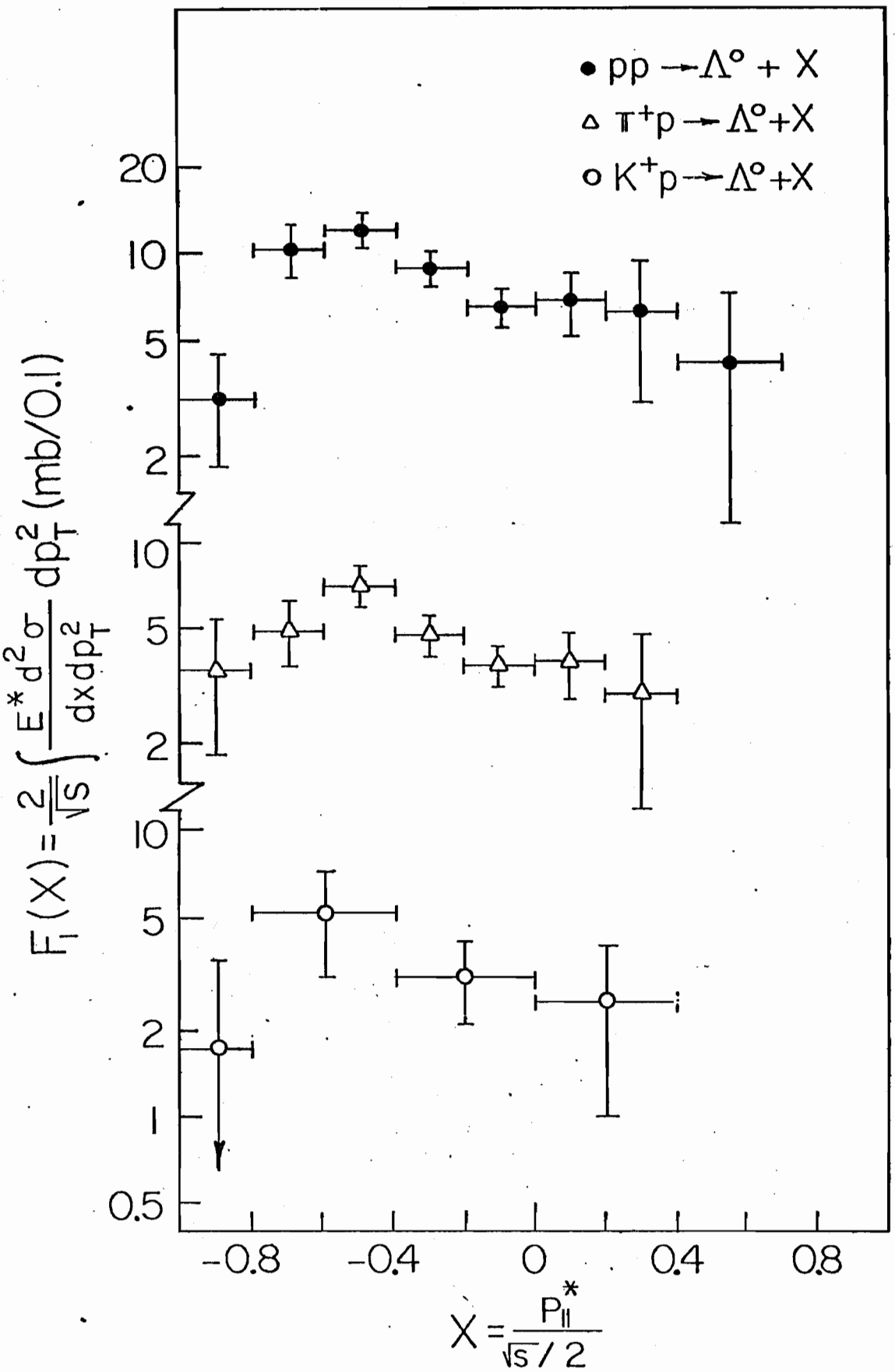
• pp → Λ° + X
△ π⁺p → Λ°+X
○ K⁺p → Λ°+X
20
10
5
2
10
5
2
10
5
2
1
0.5
-0.8
-0.4
0
0.4
0.8
$F_1(X) = \frac{2}{\sqrt{s}} \int \frac{E^* d^2\sigma}{dx\, dp_T^2} dp_T^2$ (mb/0.1)
$X = \frac{P_{\parallel}^*}{\sqrt{s}/2}$

FIG. 9

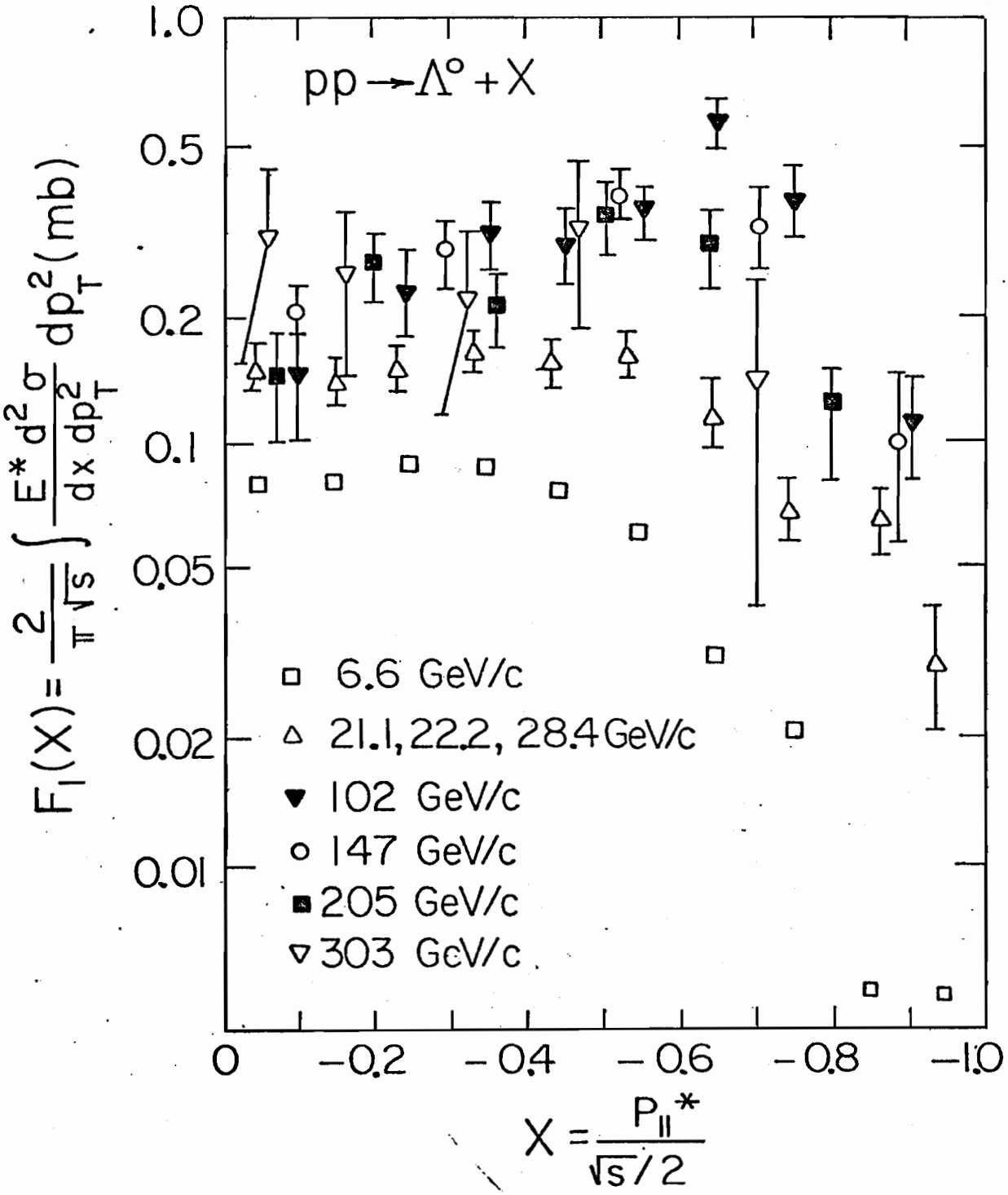
pp → Λ° + X
1.0
0.5
0.2
0.1
0.05
0.02
0.01
0
−0.2
−0.4
−0.6
−0.8
−1.0
$F_1(X) = \frac{2}{\pi\sqrt{s}} \int \frac{E^* d^2\sigma}{dx\, dp_T^2} dp_T^2 (mb)$
$X = \frac{P_{\parallel}^*}{\sqrt{s}/2}$
6.6 GeV/c
21.1, 22.2, 28.4 GeV/c
102 GeV/c
147 GeV/c
205 GeV/c
303 GeV/c

FIG. 1D

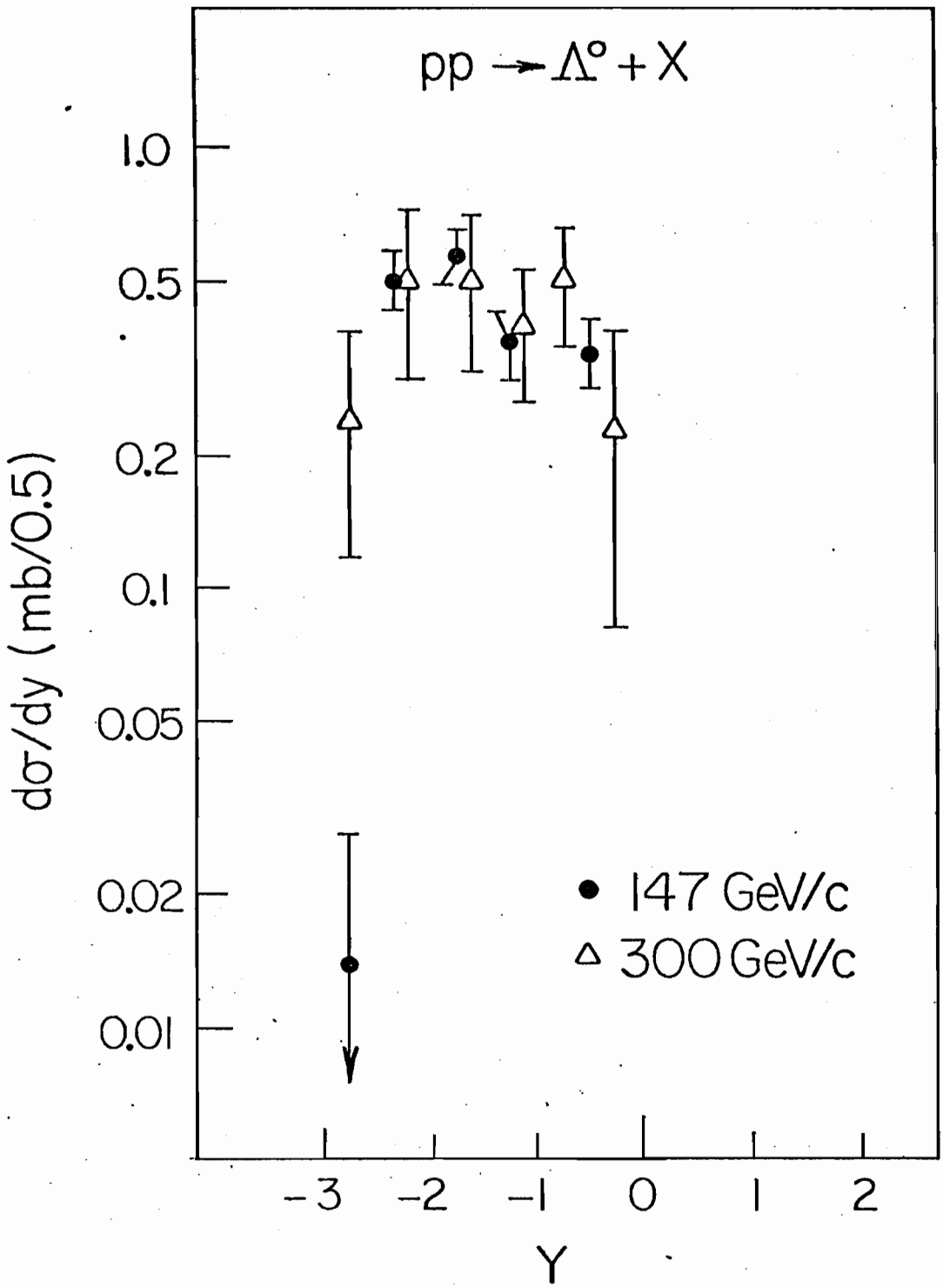
pp → Λ° + X
1.0
0.5
0.2
0.1
0.05
0.02
0.01
dσ/dy (mb/0.5)
147 GeV/c
300 GeV/c
−3
−2
−1
0
1
2
Y

FIG. 11

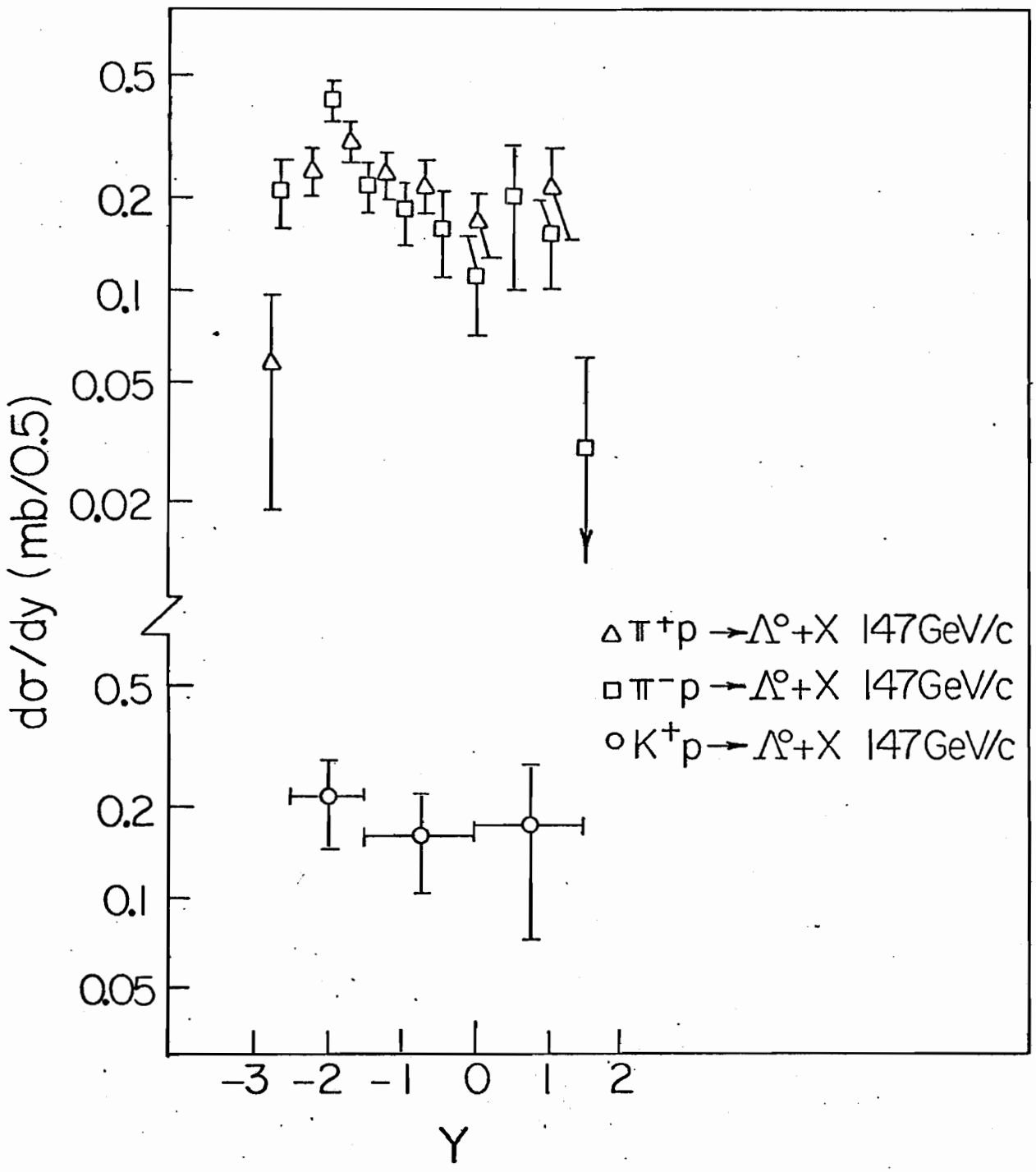
0.5
0.2
0.1
0.05
0.02
0.5
0.2
0.1
0.05
dσ/dy (mb/0.5)
△ π⁺p → Λ°+X 147GeV/c
□ π⁻p → Λ°+X 147GeV/c
○ K⁺p → Λ°+X 147GeV/c
-3 -2 -1 0 1 2
Y

FIG. 12

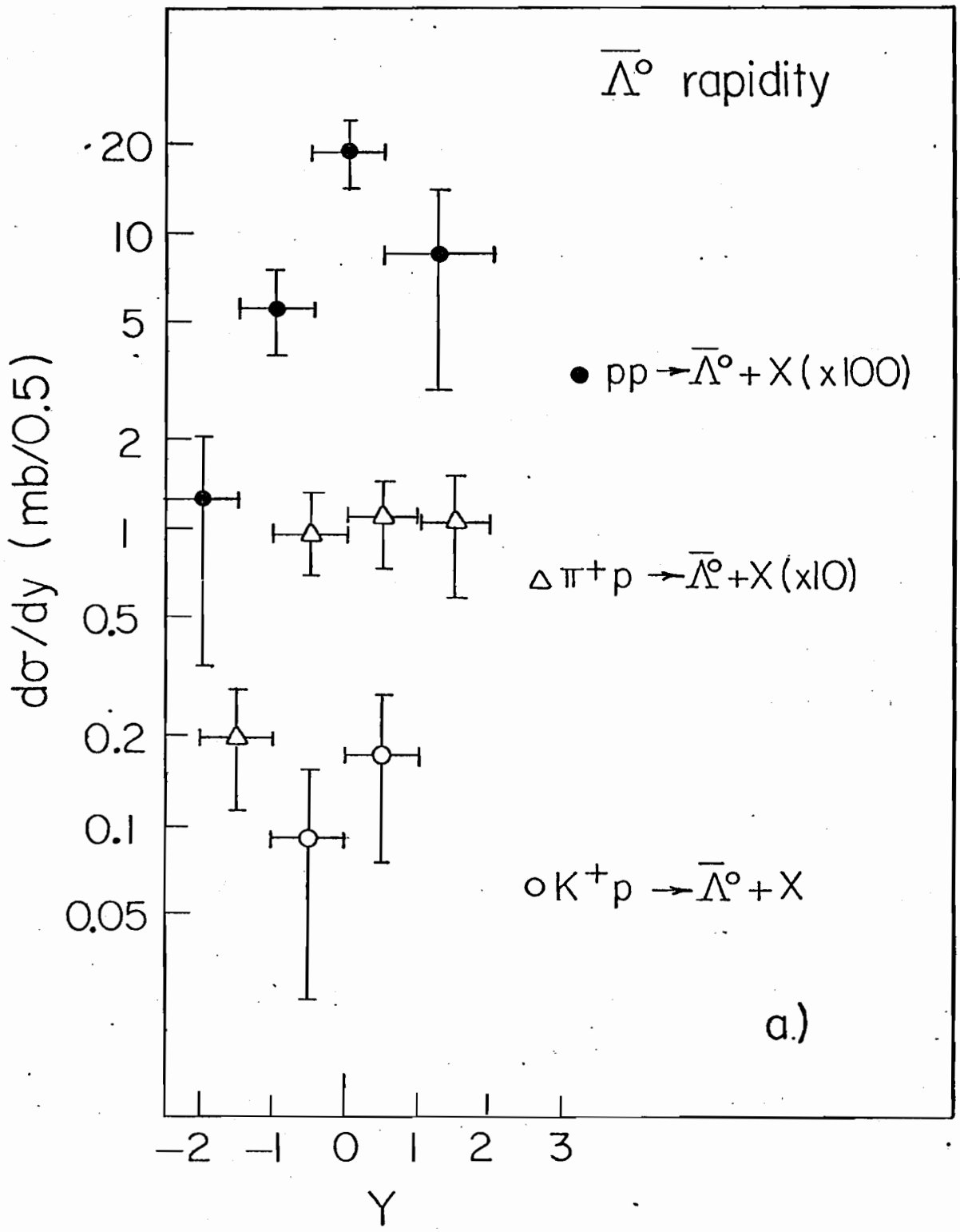
$\bar{\Lambda}^0$ rapidity
20
10
5
2
1
0.5
0.2
0.1
0.05
dσ/dy (mb/0.5)
● pp → $\bar{\Lambda}^0$ + X (x100)
△ π⁺p → $\bar{\Lambda}^0$ + X (x10)
○ K⁺p → $\bar{\Lambda}^0$ + X
a.)
−2
−1
0
1
2
3
Y

FIG. 13 (a)

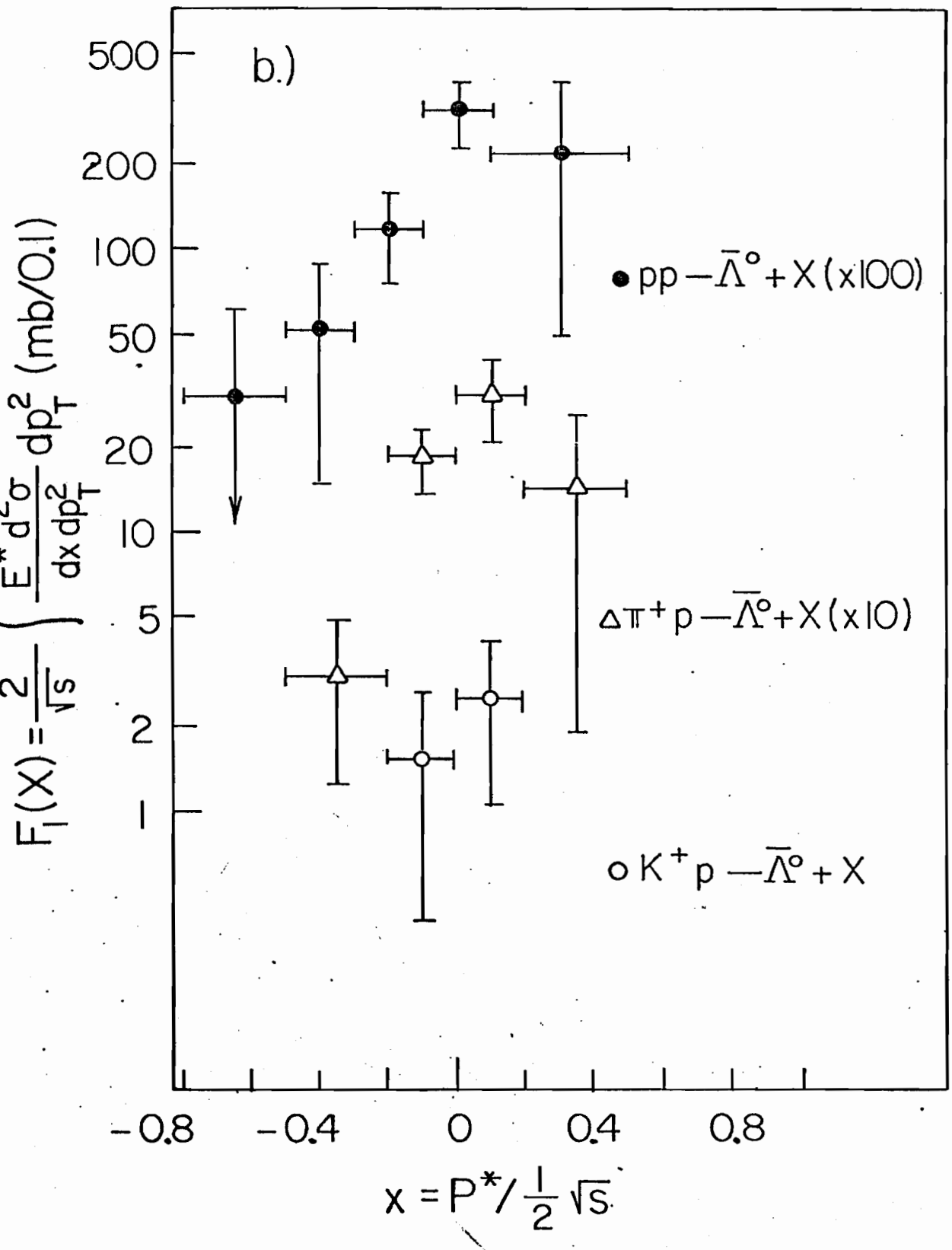
b.)
500
200
100
50
20
10
5
2
1
$F_I(X) = \frac{2}{\sqrt{s}} \int \frac{E^* d^2\sigma}{dx\, dp_T^2} dp_T^2$ (mb/0.1)
● $pp - \bar{\Lambda}^0 + X$ (x100)
△ $\pi^+ p - \bar{\Lambda}^0 + X$ (x10)
○ $K^+ p - \bar{\Lambda}^0 + X$
-0.8
-0.4
0
0.4
0.8
$x = P^* / \frac{1}{2}\sqrt{s}$

FIG. 13 (b)

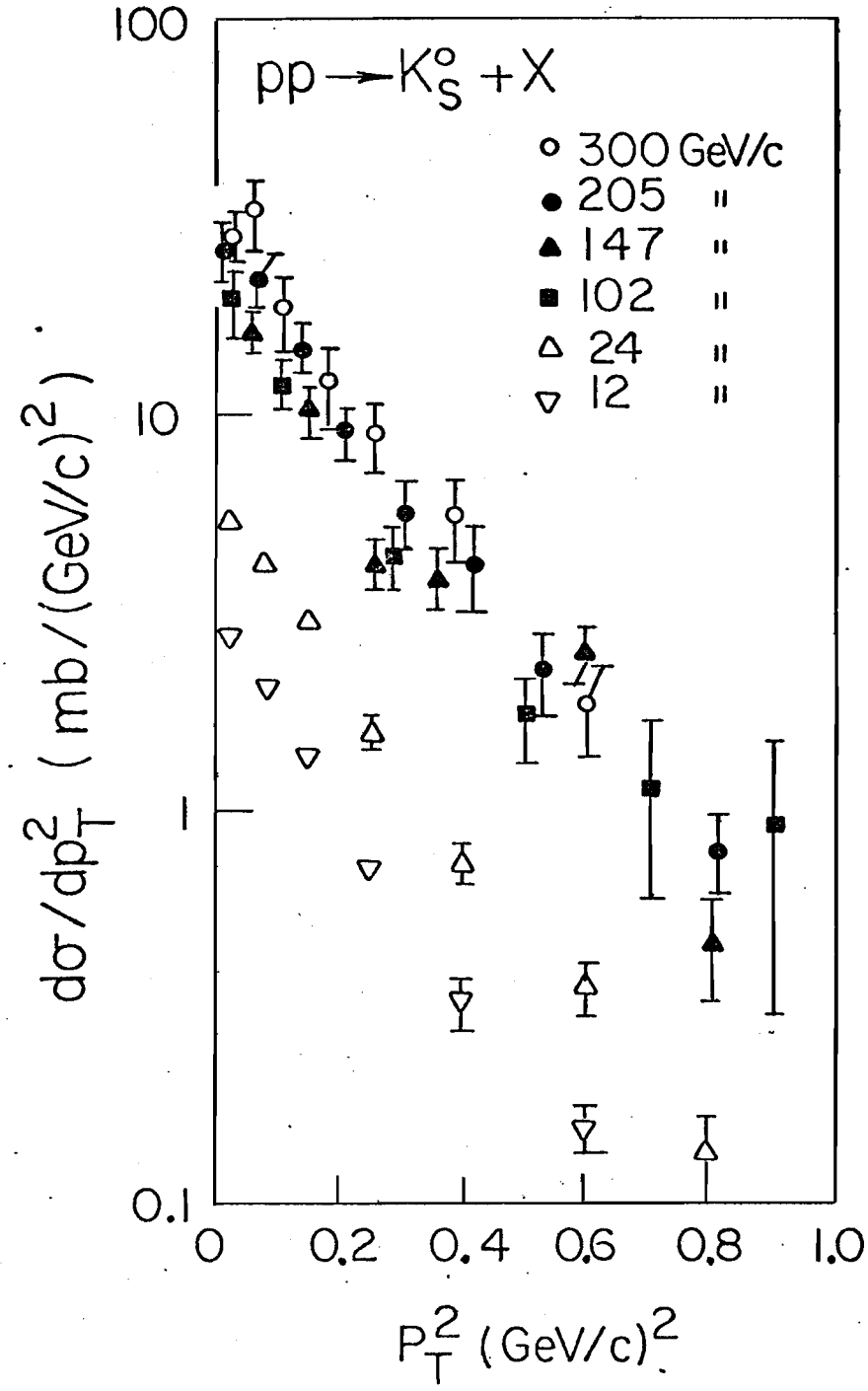
pp → K°S + X
300 GeV/c
205 "
147 "
102 "
24 "
12 "
100
10
1
0.1
0
0.2
0.4
0.6
0.8
1.0
dσ/dp²T (mb/(GeV/c)²)
P²T (GeV/c)²

FIG. 14

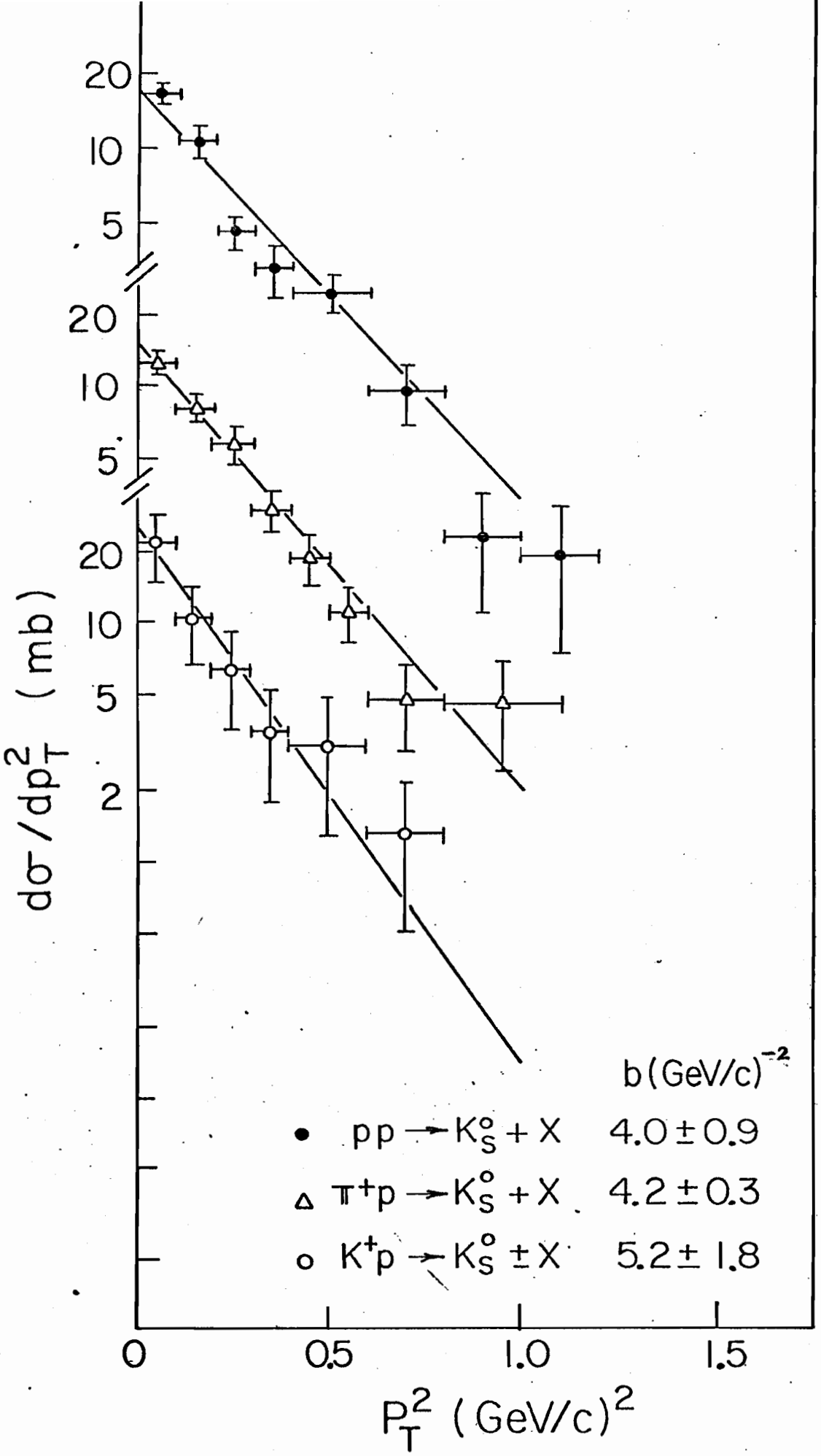
20
10
5
20
10
5
20
10
5
2
$d\sigma/dp_T^2$ (mb)
b (GeV/c)$^{-2}$
• $pp \to K_S^0 + X$ 4.0 ± 0.9
△ $\pi^+p \to K_S^0 + X$ 4.2 ± 0.3
○ $K^+p \to K_S^0 \pm X$ 5.2 ± 1.8
0
0.5
1.0
1.5
P_T^2 (GeV/c)^2

FIG. 15

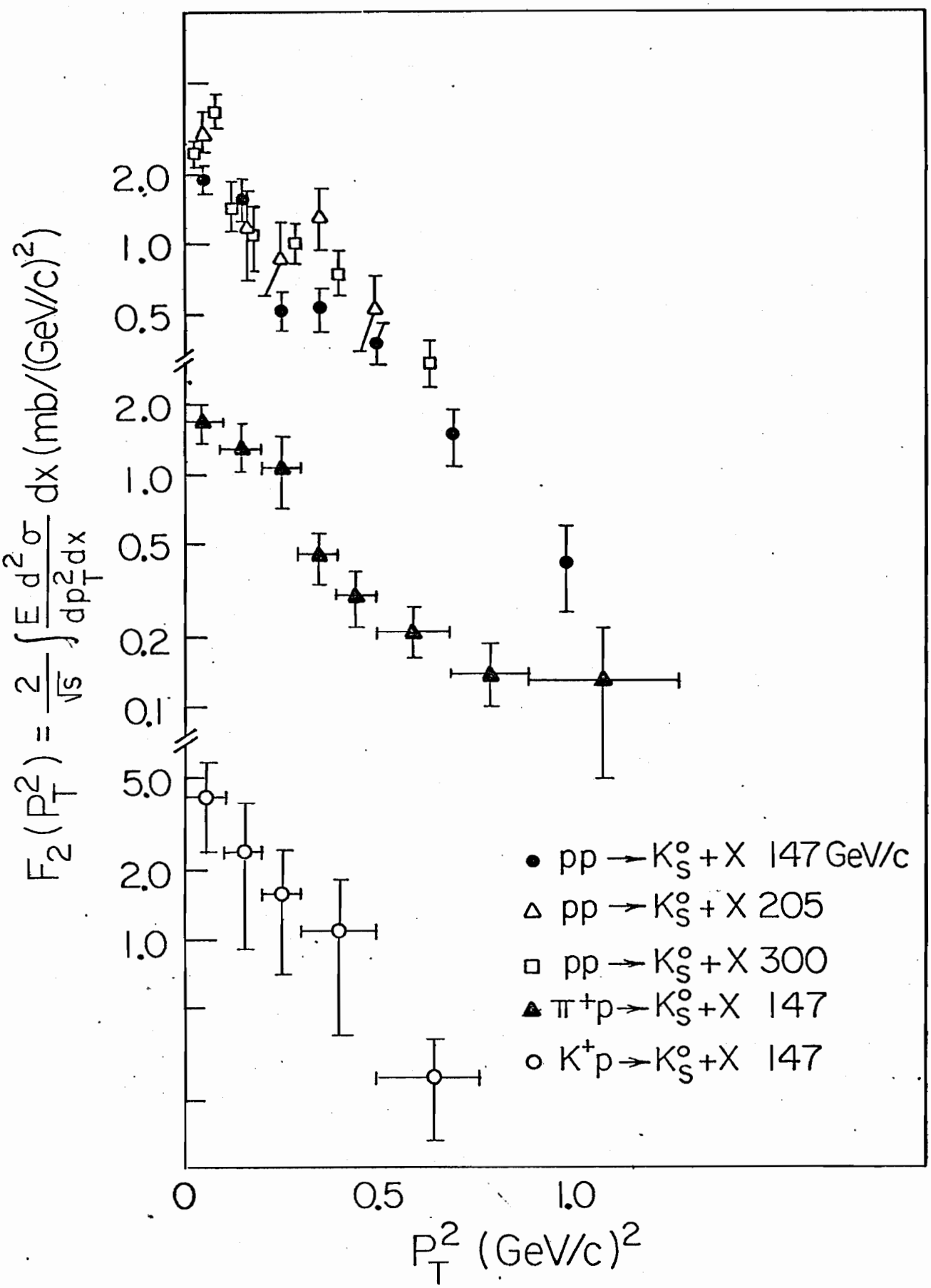
$F_2(P_T^2) = \frac{2}{\sqrt{s}} \int \frac{E\, d^2\sigma}{dp_T^2 dx} dx$ (mb/(GeV/c)^2)
2.0
1.0
0.5
2.0
1.0
0.5
0.2
0.1
5.0
2.0
1.0
0
0.5
1.0
P_T^2 (GeV/c)^2
pp → K_S^0 + X 147 GeV/c
pp → K_S^0 + X 205
pp → K_S^0 + X 300
π^+p → K_S^0 + X 147
K^+p → K_S^0 + X 147

FIG. 16

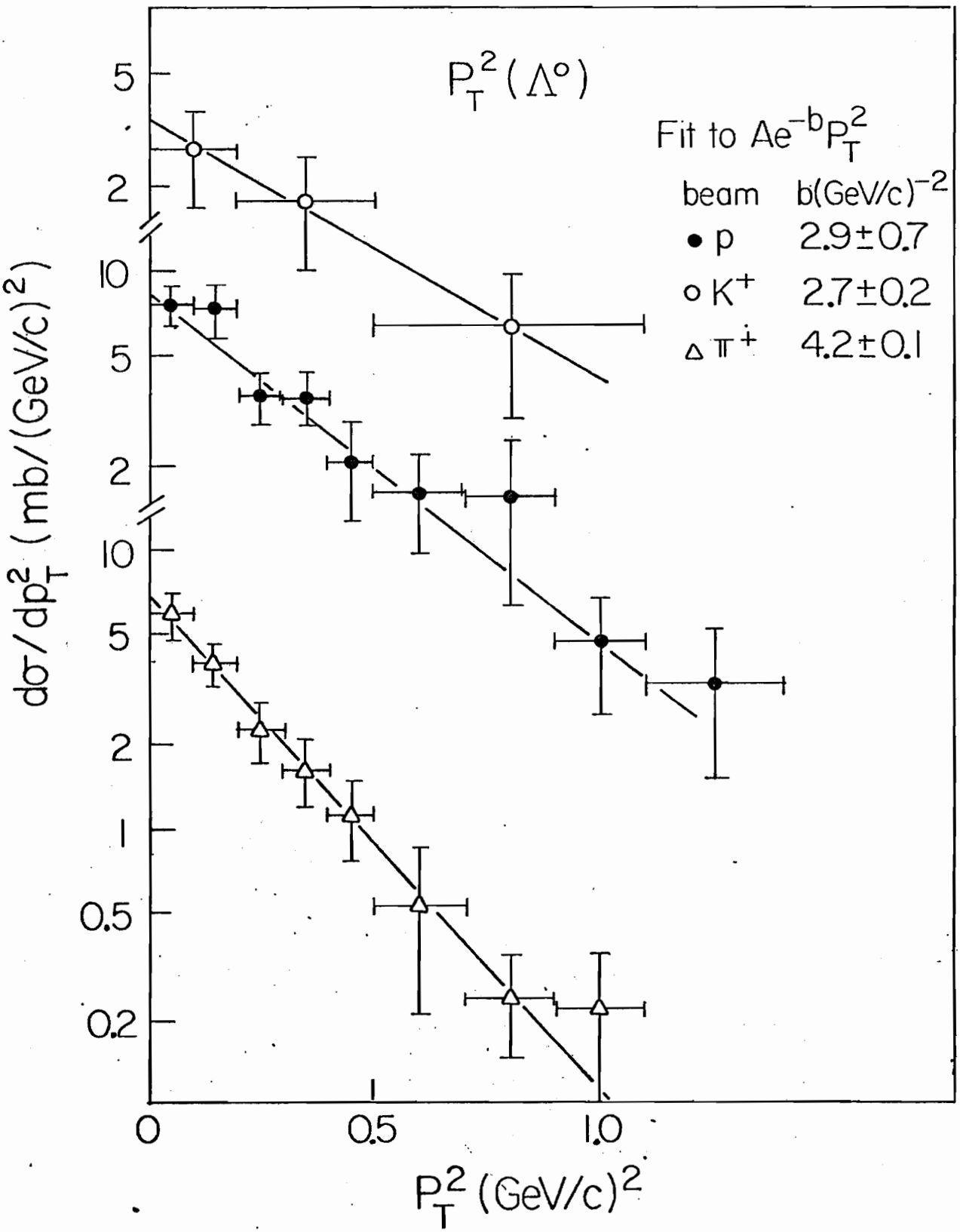
$P_T^2(\Lambda^o)$
Fit to $Ae^{-b}P_T^2$
beam b(GeV/c)$^{-2}$
• p 2.9±0.7
○ K^+ 2.7±0.2
△ π^+ 4.2±0.1
$d\sigma/dp_T^2$ (mb/(GeV/c)^2)
P_T^2 (GeV/c)^2
0
0.5
1.0
5
2
10
5
2
10
5
2
1
0.5
0.2

FIG. 17

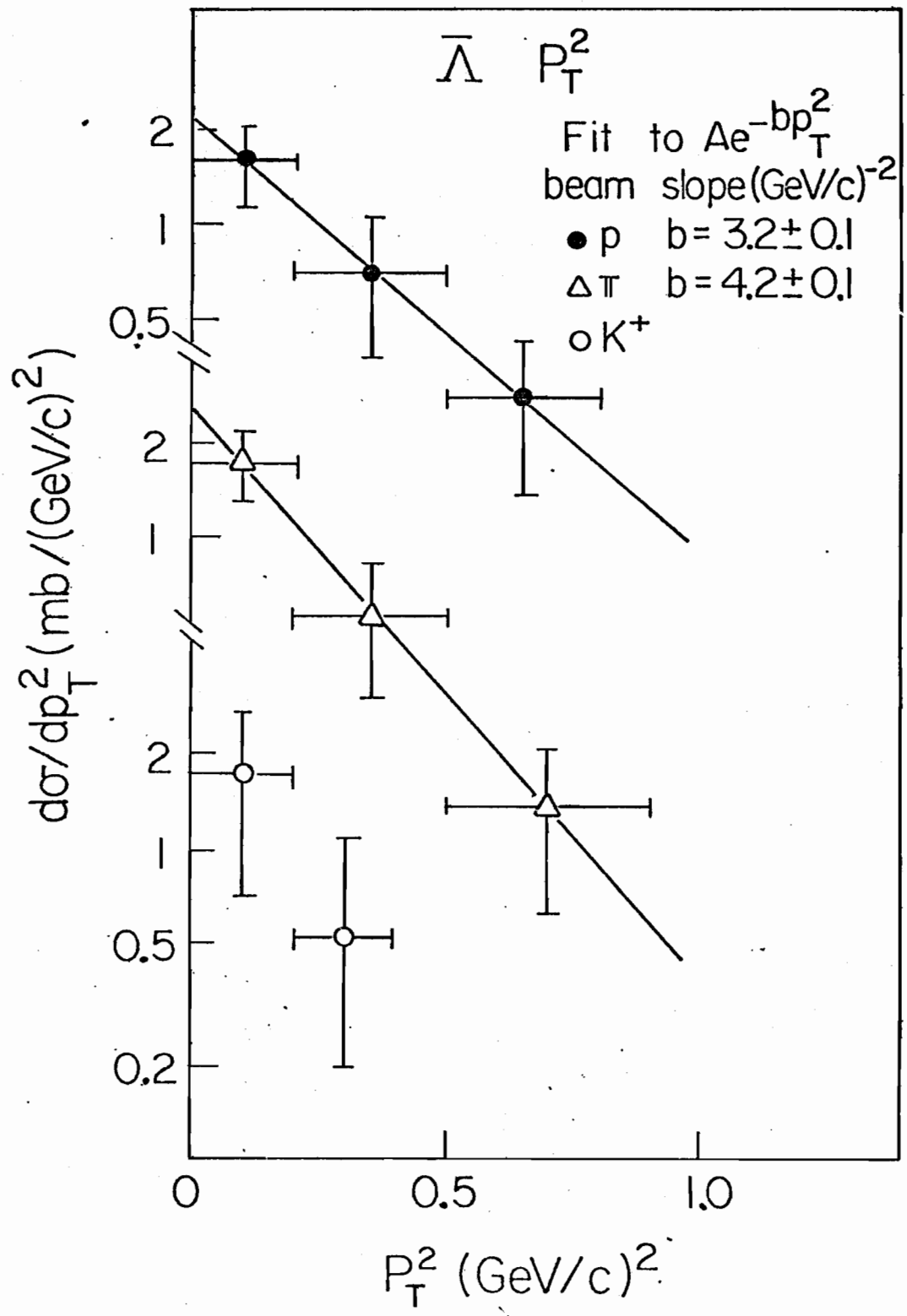
$\bar{\Lambda}$ P_T^2
Fit to $Ae^{-bp_T^2}$
beam slope $(GeV/c)^{-2}$
● p b = 3.2 ± 0.1
△ π b = 4.2 ± 0.1
○ K^+
$d\sigma/dp_T^2$ (mb/(GeV/c)^2)
2
1
0.5
2
1
2
1
0.5
0.2
0
0.5
1.0
P_T^2 (GeV/c)^2

FIG. 18